# ESA STUDY – FINAL REPORT

| | | |
|---|---|---|
| ESA Contract No:<br><br>4000117034/16/NL/NDe | SUBJECT: Simulating the cooling effect of urban greenery based on solar radiation modelling and a new generation of ESA sensors (SURGE) | INSTITUTE:<br>Institute of Geography<br>Faculty of Science<br>Pavol Jozef Šafárik University in Košice |
| ESA Contract No:<br>4000117034/16/NL/NDe | No. of Volumes: 1<br>This is Volume No: 1 | INSTITUTE'S REFERENCE:<br>SURGE_FR |

ABSTRACT:

Estimating heat transfer in complex urban environment is a highly demanded task for urban planning as the contemporary climate changes on global scale. Urban greenery has a considerable effect on cooling the urban environment during heat waves. Sentinel 2 (S2) mission could become a potential means for quantified assessment of different urban scenarios where vegetation plays essential role as the S2 data provide higher spatial and temporal resolution than is enabled by other similar missions. This feasibility study aimed to exploit the potential of S2 in simulating the cooling effect of urban greenery. The main objective was to define a methodical approach for spatial modelling of land surface temperature based on modelling the solar irradiation and parameterizing the land cover properties from S2 data. While solar irradiation can be precisely calculated on a fine scale using virtual 3D city models other important parameters for land surface temperature modelling are difficult to ascertain, such as surface thermal emissivity, broad-band albedo and evapotranspiration. The approach was tested in an area comprising 4 sq. km of the central part of the Košice City in Slovakia. Virtual 3D city model of was generated from airborne lidar and photogrammetric data acquired in a single mission. A time-series of Sentinel 2 data was gathered to be compared with a reference time-series of terrestrial lidar (TLS) data of urban greenery on 4 small sites. Statistical linear relationship was defined between the vegetation metrics derived from Sentinel 2 and TLS data. A geobotanical database of urban trees was generated based on field survey. Algorithmic structure of a toolbox for modelling the land surface temperature in the open-source GRASS GIS was developed based on the Stefan-Boltzmann law and Kirchhoff rule. This study demonstrated how Sentinel 2 data can be used for estimating broad-band albedo, land surface emissivity and solar transmittance of vegetation. The primary benefits are in the developed algorithm for estimating the land surface temperature in a GIS environment providing a unique platform (i) for integrating various kinds of datasets to become usable in urban planning and (ii) for exploitation of the Sentinel 2 data in mitigation of the urban heat island.

The work described in this report was done under ESA PECS Contract. Responsibility for the contents resides in the author or organisation that prepared it.

Names of authors: Jaroslav Hofierka, Michal Gallay, Ján Kaňuk, Vladimír Sedlák, Katarína Onačillová, Ján Šašak, Jozef Šupinský, Alena Gessert

| | |
|---|---|
| ESA PECS PROGRAMME MANAGER:<br>Kay Van Der Made<br>DIRECTORATE: IPL-ISP | |

# Simulating the cooling effect of urban greenery based on solar radiation modelling and a new generation of ESA sensors (acronym SURGE)

## Final Report

# 1 Introduction

## 1.1 Contractual

This Final Report (FR) document has been issued by the Institute of Geography, Faculty of Science Pavol Jozef Šafárik University in Košice, Slovakia (UPJS) for ESA under the PECS contract 4000117034/16/NL/Nde of the proposal SURGE (SK1-04).

**The aim of the project** was to evaluate the feasibility of joint use of virtual 3D city models and multispectral satellite imagery for approximating the dynamics of land surface temperature via modelling the spatial distribution of solar irradiation and land cover properties in a complex urban environment.

**The main objective** was to define a methodical approach for spatial modelling of land surface temperature based on modelling the solar irradiation and parameterizing the land cover properties from S2 data. While solar irradiation can be precisely calculated on a fine scale using virtual 3D city models other important parameters for land surface temperature modelling are difficult to ascertain, such as surface thermal emissivity, broad-band albedo and evapotranspiration. The approach was tested in an area comprising 4 sq. km of the central part of the Košice City in Slovakia.

Information about the project and its main results are summarized also on the website http://esa-surge.science.upjs.sk.

## 1.2 Purpose of the document

This document provides information on the main achievements of the SURGE project, grouped into five thematic technical domains. In summary:

- Review of the state-of-the-art in deriving vegetation metrics from multispectral satellite data for characterizing solar radiation transmittance of urban greenery and applicability of Sentinel 2 multispectral satellite imagery for such purposes.
- Analysis of urban heat island in the Košice City as the model area used in this study.
- Generating a high-resolution virtual 3-D city model
- Methodical approach of monitoring urban trees as a time series of 3D terrestrial laser scanning data to define their correlation with vegetation metrics derived from the Sentinel 2 multispectral satellite imagery;
- Novel algorithm of spatial distributed and physically based modelling of land surface temperature in GIS (proof-of-concept) exploiting the potential of Sentinel 2 imagery and the virtual 3D city model for simulating the cooling effect of urban greenery in a GIS environment (proof-of-concept). Road map for validation and implementation of the algorithm.

The report also explains the management of the activity and future perspectives of the results.

## 1.3 Definitions, acronyms and abbreviations

ALS Airborne Laser Scanning

AOI Area of interest

DSM Digital surface model

DTM Digital terrain model

EO Earth Observation

ESA European Space Agency

EVI Enhanced Vegetation index

GIS Geographic Information System

GRASS Geographic Resources Analysis Support System

L8 Landsat 8

LoD2 level of detail 2 of the buildings in the 3D city model

LST Land Surface Temperature

NDVI Normalized Difference Vegetation Index

S2 Sentinel 2

UHI Urban Heat Island

TLS Terrestrial Laser Scanning

## 2 Study area and data

The SURGE project was elaborated on the case study of Košice which is a typical small post-communist Central European city which has underwent considerable changes of urban landscape induced by transition to capitalism and modern trends in economy (Fig. 1). It is the second largest city in Slovakia with almost 240 000 inhabitants. The project team is based in this city therefore it was meaningful to establish the study on an area within Košice. We selected an area of a feasible size and with sufficient diversity of urban greenery which would be suitable for ground-based mapping, airborne survey and large enough for monitoring by Earth observation satellites such as Sentinel 2A and Landsat 8. As a result, the area of interest covers a rectangular area (4 km$^2$) of the central part of the city (Fig. 4) comprising various types of urban greenery and built-up areas, such as parks, alleys, greenery in residential zones. The overview of acquired types of data is shown in Fig. 2.

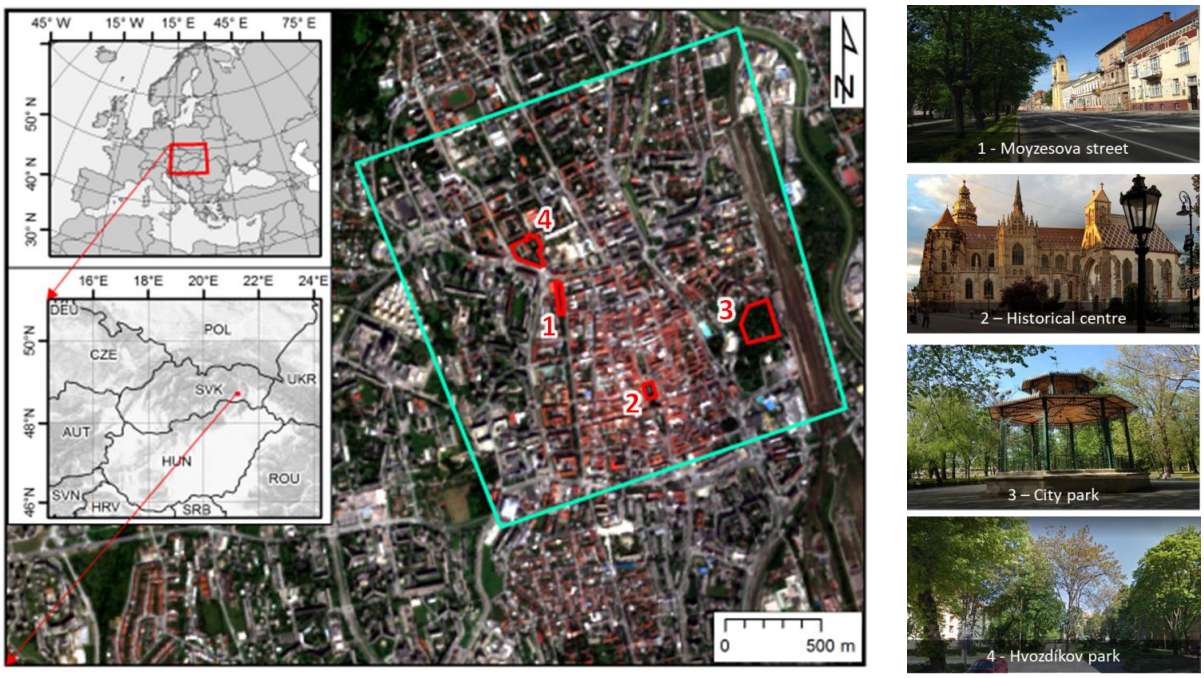


*Figure 1. Location of the study area in the Košice City, Slovakia. The cyan line outlines the area subject to airborne lidar and photogrammetric mapping in a single mission, time series of the Sentinel 2 image coverage. The red outline delineates four sites selected for repeated terrestrial laser scanning of urban vegetation. The background maps are © Copernicus, Sentinel 2A image acquired on 7 September 2016.*

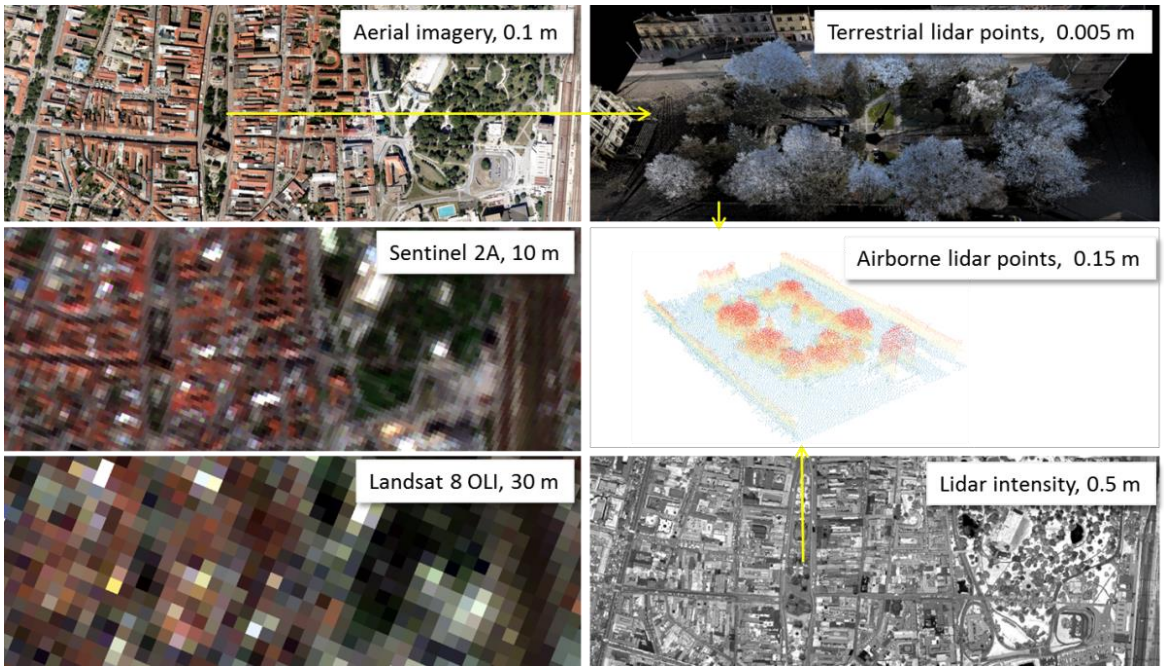


*Figure 2. Overview of the acquired spatial data for the study area and associated spatial scales. The images show the central part of the Košice City, Slovakia.*

Figure 3 and 4 show the coverage of the study area by the Sentinel 2 and Landsat 8 satellite scenes. A time-series of cloud free multispectral imagery of Sentinel 2A and 2B (https://scihub.copernicus.eu/) and Landsat 8 OLI/TIRS (https://earthexplorer.usgs.gov/) was gathered for the year of 2016 and 2017. The original S2 and L8 data was georeferenced in WGS 84 UTM projection system, Zone 34 (EPSG: 32634). The summary of data is provided in SURGE_PR1 (2016). Sentinel 2A (S2A) data was the main source of multispectral imagery for the SURGE project. The assembled time series enabled to demonstrate change of vegetation coverage by the means of true colour composites, near-infrared colour composites, and NDVI (Fig. 5). The L8 data were used for analysing the urban heat island phenomenon of in Košice which is described in Section 4.

Mapping the study area in higher resolution was deployed in the large area of displayed in cyan outline in Fig. 1. Airborne photogrammetry and airborne laser scanning (ALS) were performed in two single missions in late summer of 2016. ALS data and photogrammetric imagery were used for creation of 3-D city model consisting of buildings and terrain. We have selected four smaller test sites covering hectares (Fig. 2, red outlines) for detailed mapping of urban vegetation and its geometric change using repeated terrestrial laser scanning (TLS). Each site represents typical urban greenery consisting of various kinds of trees of different height. The data were acquired in WGS 1984 and transformed into the Slovak national projection coordinate system JTSK03 and Baltic altitude height system after adjustment (Bpv) (EPSG: 5514). Section 5 describes the 3D city model and Section 6 the TLS survey of urban greenery.

All the mentioned types of data were involved in developing the approach for simulating the cooling effect of urban greenery which is described in Section 6.

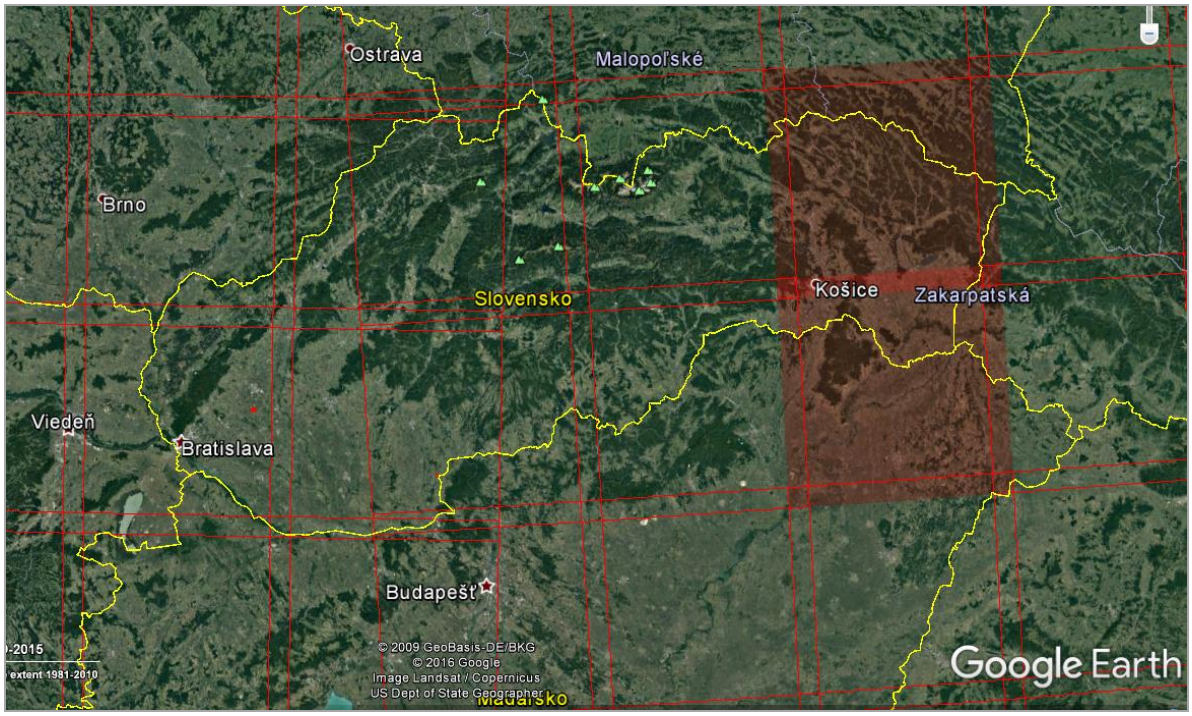


*Figure 3. The study area is situated within two Sentinel 2A data granules (34 UEU, 34 UEV).*

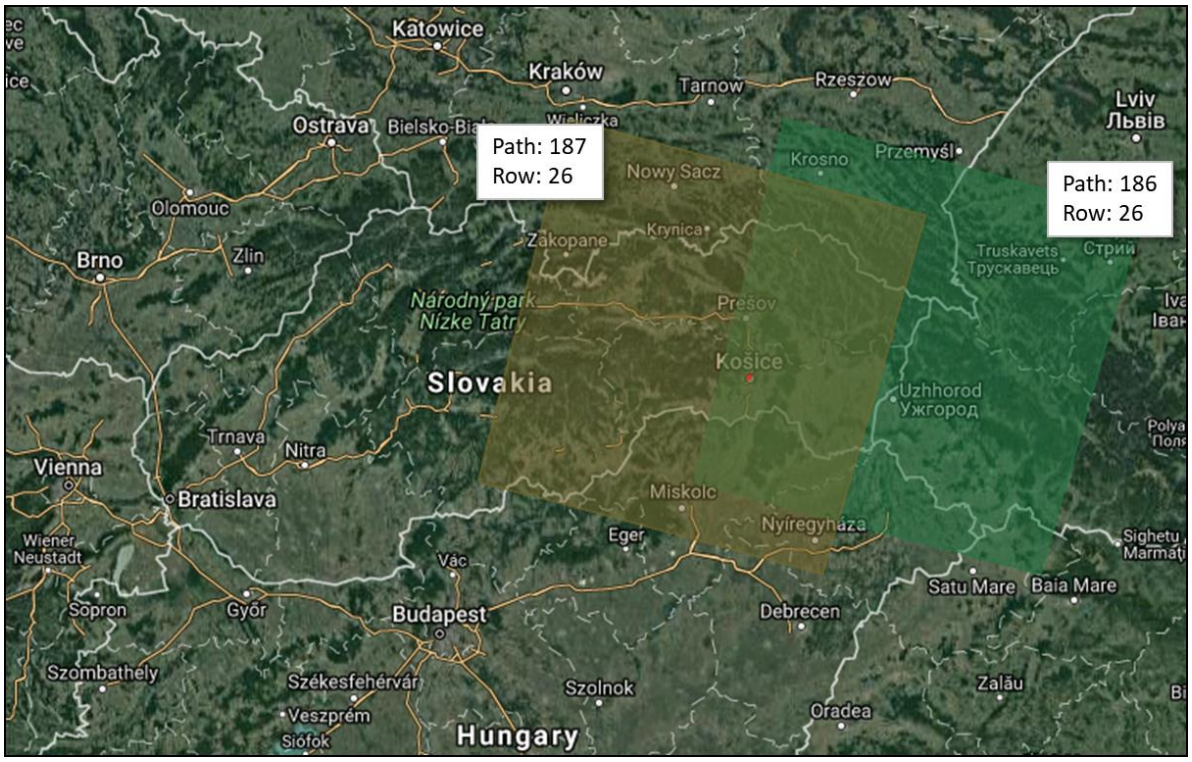


*Figure 4. The study area is situated within two Landsat 8 data scenes (186/26,187/26). Background map data © 2017 GeoBasis DE/BKG (© 2009, Google Imagery © 2017 Terra Metrics.*

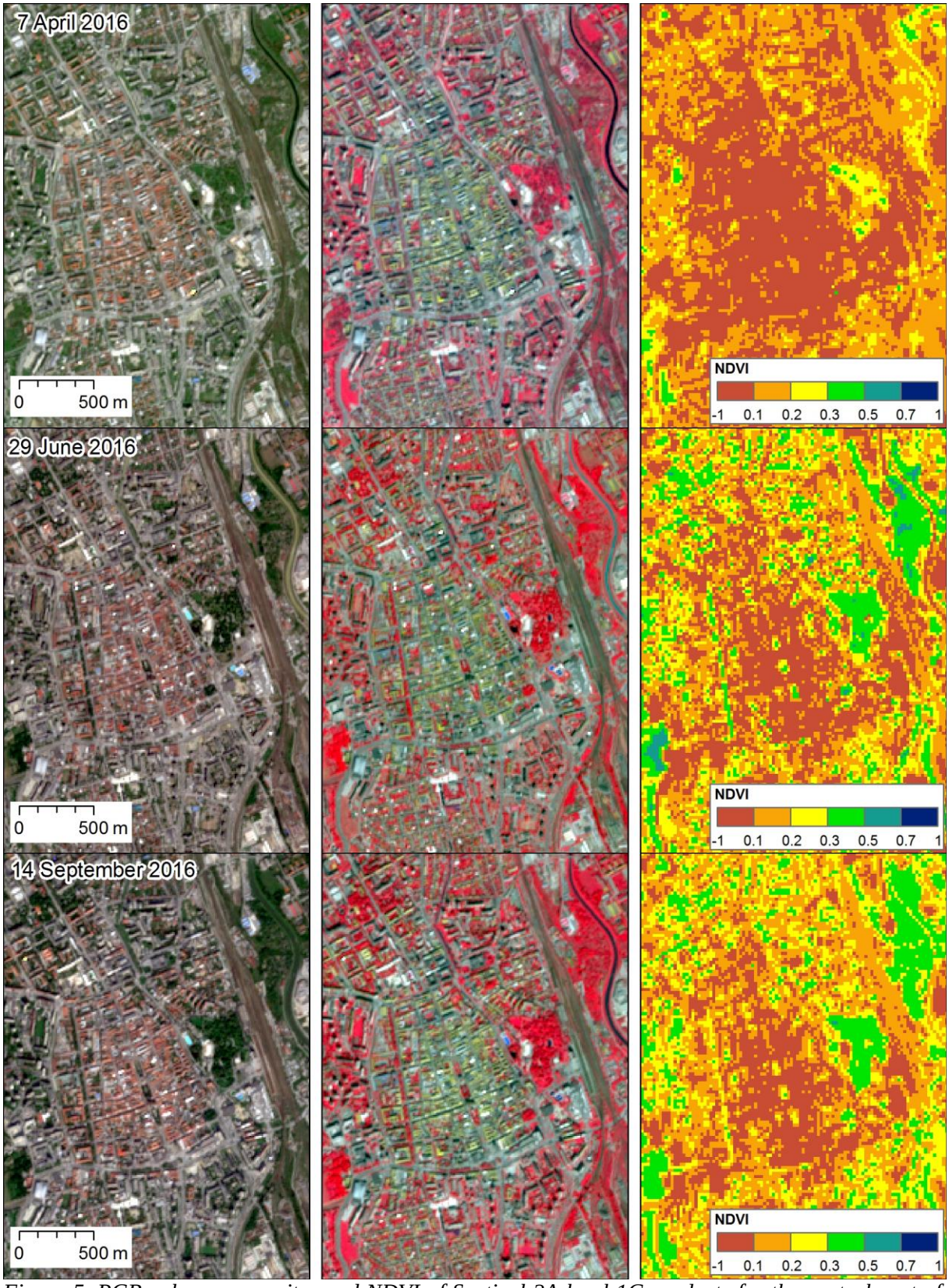


*Figure 5. RGB colour composites and NDVI of Sentinel 2A level 1C products for the central part of the Košice City. True colour image (left, bands 4, 3, 2), NIR composite image (middle, bands 8, 4, 3), NDVI (right, calculated from bands 5, 6).*

# 3 Applicability of multispectral satellite imagery for characterizing solar radiation transmittance of urban greenery

Urban greenery has various positive micro-climate effects including mitigation of heat islands. The primary root of heat islands in cities is in absorption of solar radiation by the mass of building structures, roads and other solid materials. The absorbed heat is subsequently re-radiated into the surroundings and increases ambient temperatures. The vegetation can stop and absorb most of incoming solar radiation mostly via the photosynthesis and evapotranspiration process. Given the associations between vegetated land cover and the biophysical and social processes of urban systems there exists an ongoing demand for effective urban vegetation mapping and classification techniques (Tooke et al., 2009). The results of the study by Tooke et al. (2011) indicated that trees on average reduce 38% of the total solar radiation received by residential building rooftops. Fogl and Moudrý (2016) found lower effect in the range of 3 - 11% and note that over 50% of the solar radiation loss occurs during the summer time. Radiation received at the urban surface is highly variable in space and time resulting from the complex form and land cover of urban environments. Understanding this variation in intercepted solar radiation is fundamental to determining various components of the urban energy landscape. Multispectral imagery acquired by space borne sensors is a key data source for earth monitoring programs considering the great advantages that they have.

Therefore, in the initial stage of the SURGE project, we summarized the published research (state-of-the-art) on derivation of vegetation metrics from multispectral satellite data for characterising the solar radiation transmittance of urban greenery (SURGE_D1_SOA_MSVT). We focused on the applicability of the Earth Observation sensors which are currently in operation and which provide high resolution in spectral and spatial domain with a high frequency of sensing repetition over the same area. In addition the data should be accessible free of charge via internet. Such data is easily obtainable via internet connection to produce and update vegetation inventories over large regions if aided by satellite imagery and appropriate imagery analysis. The review showed that the most widely used sensors from this perspective comprise those of the Landsat mission (TM, ETM+, OLI, TIRS), and further MODIS, ASTER, MERIS, SPOT, IKONOS. Another advantage is in the high temporal resolution (short revisit period over the same area) ranging between days to few weeks.

A growing number of studies have examined a wide variety of vegetative phenomena, including mapping vegetation cover, by using remote sensed data. Various techniques were developed to associate spectral response of the land cover surface with biophysical and structural properties of vegetation. In particular, combinations of red and near infra-red bands were used to derive vegetation indices (Table 1, 2) which were proved to be correlated with particular vegetation metrics such as leaf area index, canopy gap fraction, canopy closure, etc. The most popular is the normalized vegetation index (NDVI), which is simple to calculate and provides a proxy for calculating metrics which are difficult to be measured directly from the satellite imagery, such as such as leaf area index (LAI), canopy cover and gap fraction.

Our study focuses on associating spectral response of the land cover recorded by the ESA Sentinel 2A satellite and solar transmittance modelled by high resolution lidar data of urban

greenery. The presented review of the contemporary state-of-the art showed that similar tasks were addressed mainly by published studies focusing on forested areas and applications in forestry, some in urban environment. In principle, the strength of the relationship between the information derived from multispectral imagery and the data used as the ground truth of vegetation transmittance strongly depends on the spectral and spatial resolution of the imagery. From this point of view the Sentinel 2A products have potential to provide more accurate estimates of the vegetation transmittance given higher number of spectral bands and higher spatial resolution of some bands in comparison with similar other Earth observation sensors (e.g. Landsat 8 OLI, Landsat 7 ETM+, ASTER, MODIS). This was proven by several studies prior to the launch of Sentinel 2A which used simulated bands.

# 4 Urban heat island in the Košice City, Slovakia

The availability of multispectral imagery including a thermal infrared band enabled monitoring the spatial pattern of land surface temperature (LST) and linking it with land cover properties. Multispectral data archives allow for assessing the dynamics of urban heat island (UHI) by the means of LST mapping for particular area. Many studies demonstrated the existence of urban heat island (UHI) phenomenon in large cities such as Berlin, London, Moscow, Beijing, but only few studies focused on small cities of several hundred thousands of inhabitants. Landsat 7 and Landsat 8 missions provide valuable multispectral imagery which we used to conduct spatio-temporal analysis of land surface temperature (LST) in Košice in recent years.

The whole administrative area was subject to analysis of the UHI phenomenon in the city (Fig. 6, 7) and the results were summarized in Onačillová and Gallay (2018). Košice experience higher LST in the built-up areas than in the surrounding landscape comprising forests or grassland which provides evidence of the UHI phenomenon in the city.

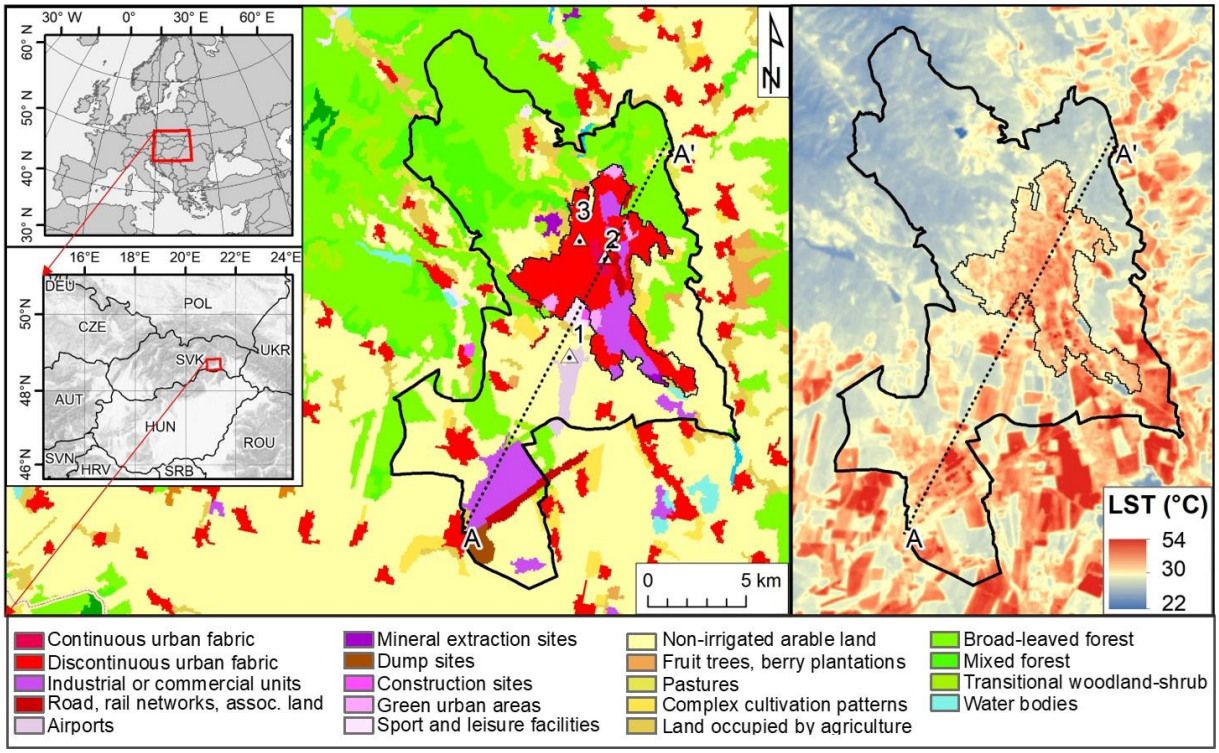


*Figure 6. Location of the Košice City as the administrative area (thick black solid line) and urbanized core (thin black solid line) overlaid on CORINE Land Cover 2012 and land surface temperature (LST) 6 August 2015 with the meteorological stations at the airport (1), city centre (2), and at the Technical University in Košice (3). Vertical profile along the line A-A' is displayed in Fig. 7.*

Given the analysed period between March and November, UHI is most pronounced in the summer. Clear positive strong correlation was found between the air temperature and the LST based on the analysed LST datasets and three weather stations. LST was found to be in a strong negative correlation with NDVI (Fig. 8) in the growing season when plants have high chlorophyll content. Even small areas such as tree alleys or small gardens and parks with green vegetation within the urban fabric can mitigate the LST (Fig. 9).

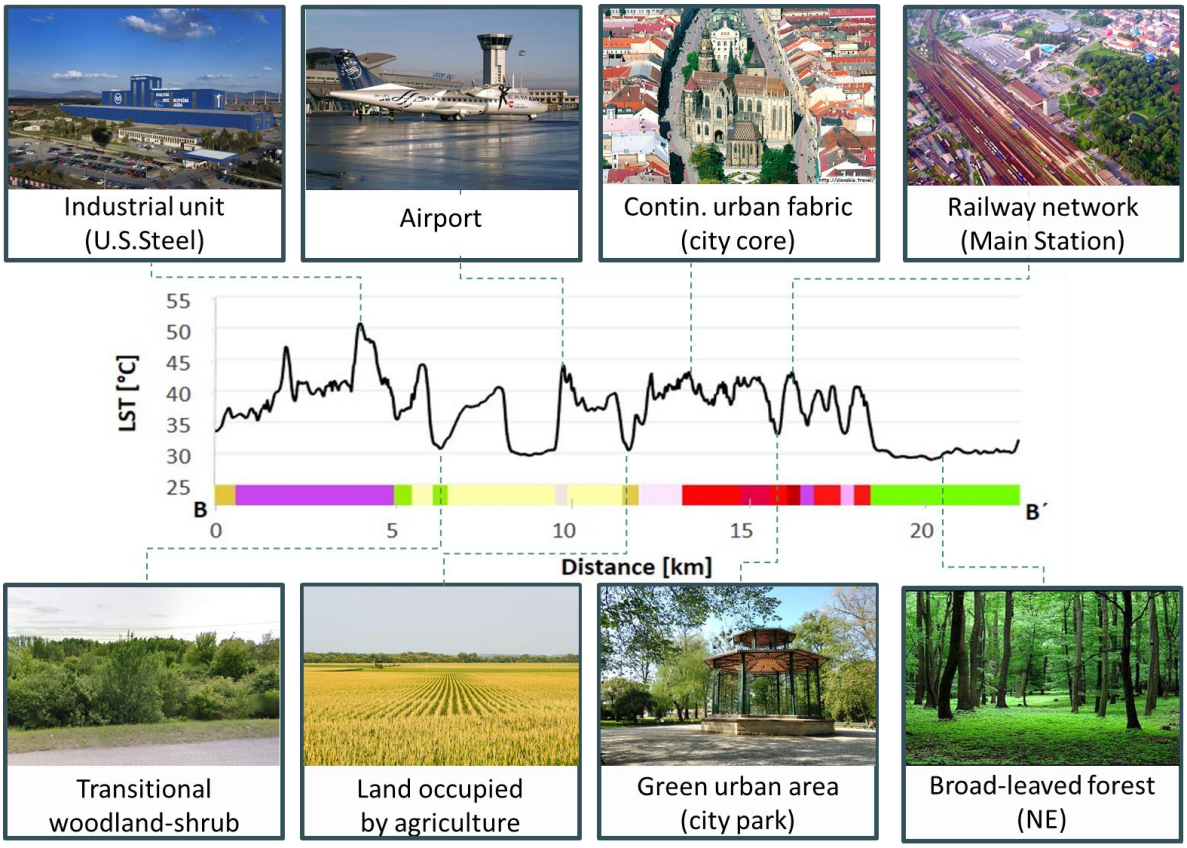


*Figure 8. Vertical cross-section profile of the LST surface derived from the Landsat 8 TIRS Band 11 (6 August 2016) with the CORINE Land Cover 2012 classes crossed along the line B-B' shown in Fig. 16 demonstrating how impervious land cover and green areas influence the urban heat island.*

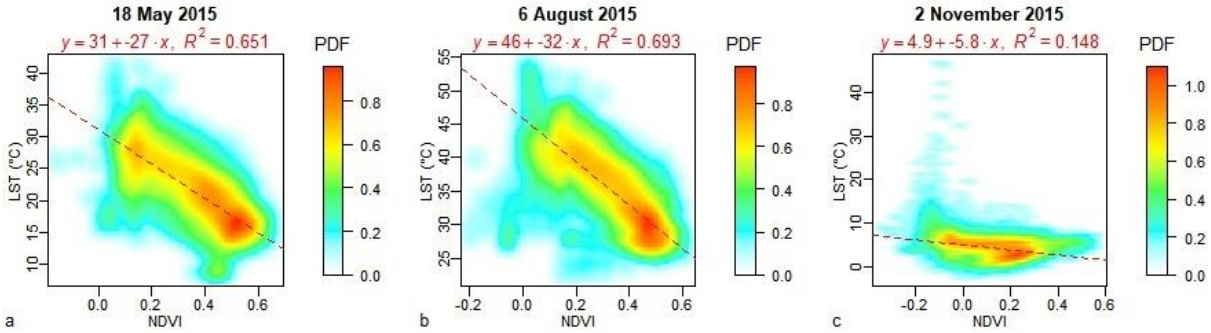


*Figure 9. Smoothed scatterplots of LST and NDVI in the administration area of Košice for three selected dates in spring, summer and late autumn. For high density of points in the scatterplots, the points are expressed as the values of probability density function (PDF) resulting from a two-dimensional kernel density estimation. Each scatterplot comprises a linear regression model. Adopted from Onačillová and Gallay (2018).*

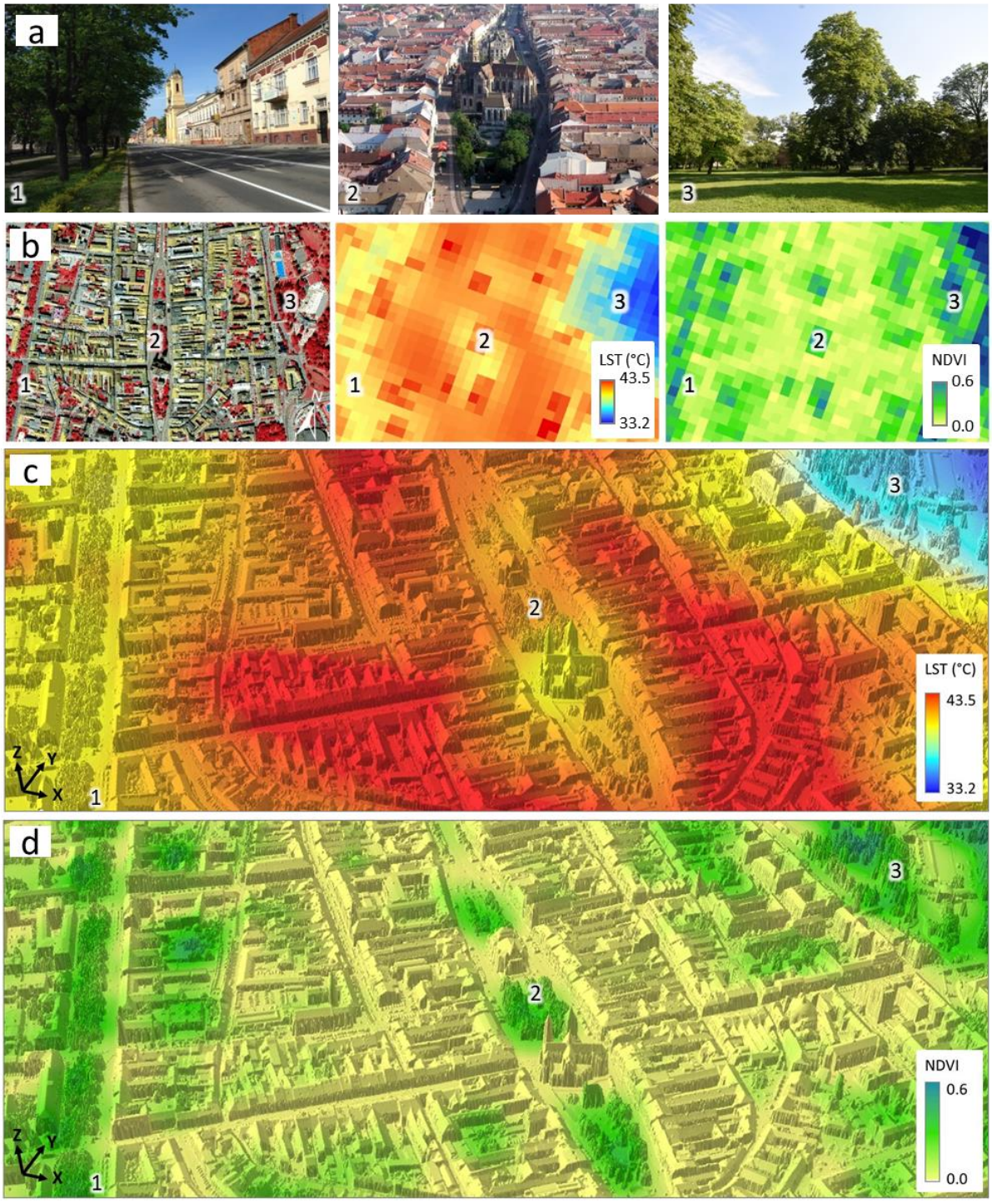


*Figure 3. LST and NDVI values on 6 August 2015 in selected areas of the historical city centre of Košice (A): 1 – green alley on Moyzesova Street, 2 – the core of the city-centre, 3 – city park. (B) perspective 3D view of the LST model resampled to 0.5 m resolution draped over the lidar based digital surface model described in Hofierka et al., (2017). Figure is adopted from Onačillová and Gallay (2018).*

The results provided several examples that replacing semi-natural grassland or agricultural land for new shopping centres, commercial zones or industrial parks in the last two decades amplified the UHI effect and contributed to its expansion into suburban zones. Elimination of the UHI effect and the effort for balanced presence of built-up areas and greenery in the further development of the city should be a priority for the upcoming years for the city management. Only in the harmony of these elements, the city can remain a full-valued environment for its inhabitants.

The study of Onačillová and Gallay (2018) suggested that the research of spatial aspects of LST in Košice or other cities could exploit the advance of new earth observation satellite missions, such as Sentinel 2. This mission provides higher spatial, temporal and spectral resolution in the near infrared spectral domain than the Landsat 8 data. Despite not having the thermal band, Sentinel 2 can provide higher resolution of NDVI for estimating the thermal emissivity of land cover for LST calculation from Landsat 8 TIRS thermal data.

# 5 Generating a virtual 3-D city model of the Košice City

Multispectral satellite imagery of S2 an L8 provide information on spectral properties of the land cover in relatively high resolution, but not fine enough to reliably quantify the land surface temperature in complex urban landscape. However, the main benefit is in the relatively high temporal resolution and free access to the data in comparison to more detailed alternatives such as airborne laser scanning or photogrammetric datasets. One of the hypothesis in the SURGE study was that precisely measured 3D city models can be used for calculating the incident solar energy which can be converted to land surface temperature. For that certain parameters which change dynamically over time can be estimated from the coarser multispectral satellite datasets. Therefore, a virtual 3D city model was required to address this hypothesis in the study. Custom aerial survey was procured to acquire 3D airborne laser scanning (ALS) data and photogrammetric imagery to map urban greenery over the whole study area (Fig. 1, cyan outline). Also 3-D vector models of buildings were supplied within this service. The data were used to generate a 3-D city model of the study area.

## 5.1 Airborne laser scanning data

This data were acquired in a single mission on 14 September 2016 under leaf-on conditions with a Leica ALS70-CM lidar system with other specifications listed in Table 3. The raw point data were supplied in the national cartographic projection system S-JTSK Krovak East North (EPSG: 5514) and also in UTM/WGS84. The points were processed in LAStools to classify them in ground, vegetation, buildings and other returns. Ground returns were used to derive a gridded digital terrain model (DTM) and digital surface model (DSM) of 0.2 m and 0.5 m cell size, respectively.

## 5.2 Airborne photogrammetry data

Photogrammetric imagery was collected in 4 spectral bands (blue, green, red, near infra-red) in a single mission flown on 9 August 2016 under leaf-on conditions by Vexcel UltracamXp digital camera resulting two natural and NIR false colour orthoimagery with spatial resolution of 10 cm. The photogrammetric stereo imagery was used to derive a 3-D city model

representing the buildings in the study area with LoD2 (Fig. 4). For mapping the urban greenery in the entire study area airborne laser scanning data coupled with NIR false colour photogrammetric imagery was used (Fig. 5). The ALS points representing the vegetation were extracted by classification based on point heights and by thresholding the RGB values from the NIR colour composite. For mapping the urban greenery in the entire study area airborne laser scanning data coupled with NIR false colour photogrammetric imagery was used. The airborne laser scanning (ALS) points representing the vegetation were extracted by classification based on point heights and by thresholding the RGB values from the NIR colour composite. The orthoimagery was supplied in the national cartographic projection system S-JTSK Krovak East North (EPSG: 5514) and also in UTM/WGS84.

*Table 3. Parameters of the ALS mission flown with a Leica ALS70-CM lidar system.*

| Parameter | Value |
|---|---|
| Flight height above ground | 1050 - 1087 m |
| Flight altitude above mean sea level | 1,333 m |
| Total number of points | 365 million |
| Total area | 4 $km^2$ |
| Average density of returns (all/ground) | 91 / 15 points per $m^2$ |
| Absolute overall accuracy in open areas | 0.1 m @ 1σ |


*Figure 4. Perspective 3D view of the entire study area (cyan outline in Fig. 1) for which the 3D city model was generated. 3D buildings are dispalyed on a digital terrain model in the ArcScene software by ESRI.*


*Figure 5. ALS dataset of the Košice city visualized in an interactive web interface based on the Potree renderer (Institute of Computer Graphics and Algorithms, TU Wien) and laspublish software by rapidlasso GmbH. Available at: [https://esa-surge.science.upjs.sk/laspublish/ALS_Kosice.html](https://esa-surge.science.upjs.sk/laspublish/ALS_Kosice.html)*

## 5.3 Geobotanical field survey

The city model also includes information ascertained in a geobotanical field mapping when position (latitude, longitude), plant species, basic morphological parameters and health conditions were recorded for each tree within the four smaller sites. These data helped to improve interpretation of the lidar point clouds and orthoimagery. The geobotanical survey concerned the four smaller sites for which the information is assigned to the 2-D polygon and meshed 3-D models of trees (Fig. 6). Based on the airborne photogrammetric and laser scanning data the calculated green vegetation covers about 23% of the study area. The mean height of vegetation above 0.1m is 8.4 m with standard deviation of 6 m. The highest trees reach up to 36 m but half of them is lower than 10 m. The vegetation in the four small sites that were subject to TLS survey comprises 83% of deciduous species and 17% of coniferous species. Details are provided in SURGE_D4_VEGMETR.

## 5.4 Geodatabase structure

The 3-D city model covers the entire study area which is displayed in Fig. 2 (cyan outline) and it represents the Deliverable 2 (SURGE_PR2). The 3-D city model of the entire study area is a static 3-D representation of the area valid to September 2016 when the main component of spatial data was acquired (ALS, photogrammetry). The size of the entire 3D city model is nearly 43 GB therefore the complete model is made available via URL which is described in SURGE_PR2. We generated an interactive 3D web interface for public viewing of the ALS point cloud (Fig. 6). The data of the complete model are organized in a hierarchical structure of folders (Fig. 7) which comprise data georeferenced in in the Slovak national grid system (EPSG code: 5514, in ArcGIS by ESRI: Projected Coordinate System: SJTSK_Krovak_East_North). This model contains 5 digital representations of 4 kinds of objects:

1. buildings as 3-D buildings vectors,
2. trees as ALS 3-D points, 2-D vector polygons,
3. terrain as a digital terrain model (2-D raster/grid),
4. land cover surface as a digital surface model (2-D raster/grid),
5. land cover as a digital orthoimagery in natural and false colours (2-D raster image).

In addition, the geodatabase comprises data for the four smaller sites which were subject to high resolution monitoring of vegetation 3D structure by TLS. The city models of the four smaller sites therefore contain a dynamic component, i.e. 3-D models of trees. A project file for 2-D and 3-D visualization is prepared for each of the sites (Fig. 7B). The geodatabase contains also a reduced dataset of the 3D city model. The titles of the subfolders on lower level are self-explanatory. The data are provided in standard data formats for geographic information systems software (e.g. ArcGIS, Quantum GIS) such as ESRI shapefiles or gridded raster data (TIFF, ASCII, DXF, VRML). Short description of the data in the folders is reported in a *metada.txt* file.

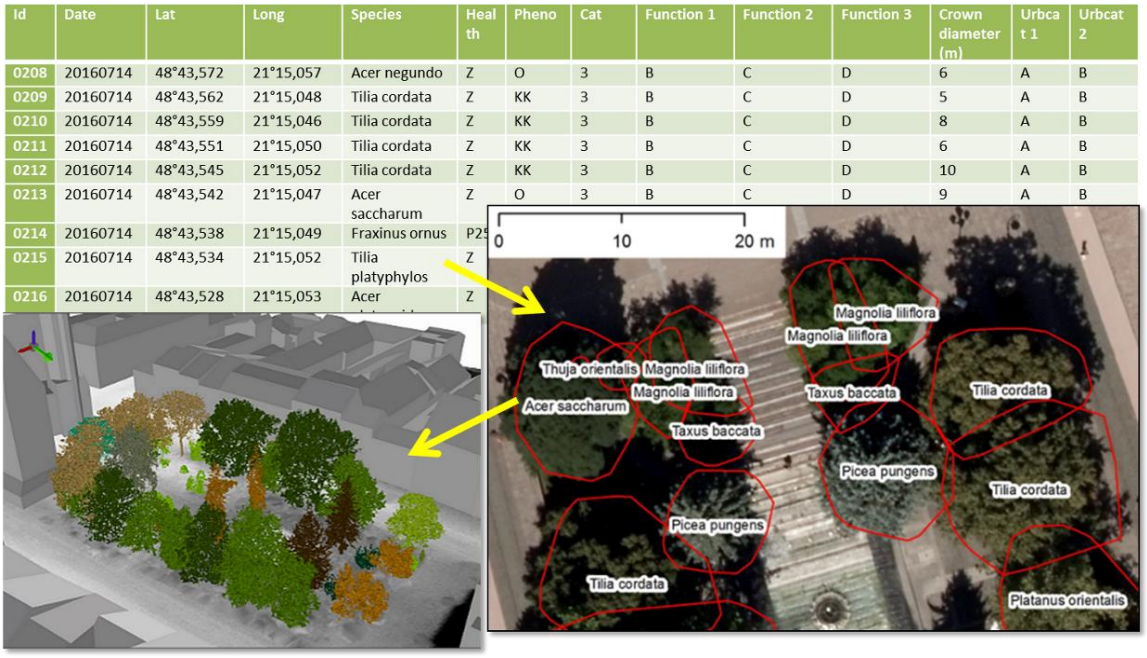

| Id | Date | Lat | Long | Species | Heal th | Pheno | Cat | Function 1 | Function 2 | Function 3 | Crown diameter (m) | Urbca t 1 | Urbcat 2 |
|---|---|---|---|---|---|---|---|---|---|---|---|---|---|
| 0208 | 20160714 | 48°43,572 | 21°15,057 | Acer negundo | Z | O | 3 | B | C | D | 6 | A | B |
| 0209 | 20160714 | 48°43,562 | 21°15,048 | Tilia cordata | Z | KK | 3 | B | C | D | 5 | A | B |
| 0210 | 20160714 | 48°43,559 | 21°15,046 | Tilia cordata | Z | KK | 3 | B | C | D | 8 | A | B |
| 0211 | 20160714 | 48°43,551 | 21°15,050 | Tilia cordata | Z | KK | 3 | B | C | D | 6 | A | B |
| 0212 | 20160714 | 48°43,545 | 21°15,052 | Tilia cordata | Z | KK | 3 | B | C | D | 10 | A | B |
| 0213 | 20160714 | 48°43,542 | 21°15,047 | Acer saccharum | Z | O | 3 | B | C | D | 9 | A | B |
| 0214 | 20160714 | 48°43,538 | 21°15,049 | Fraxinus ornus | P25 | | | | | | | | |
| 0215 | 20160714 | 48°43,534 | 21°15,052 | Tilia platyphylos | Z | | | | | | | | |
| 0216 | 20160714 | 48°43,528 | 21°15,053 | Acer | Z | | | | | | | | |



*Figure 6. Schematic work flow of assigning tree attributes from field survey to trees as 3D objects in a geodatabase. Footprint polygons of trees identified from the ALS point cloud (red outline) with assigned attributes according to the field survey overlaid on top of the aerial orthoimage. The geobotanical data is accessible also via*
*https://drive.google.com/open?id=1Pu5RdDLnkvORXlPTN7ol386vcPsO_xoP&usp=sharing*

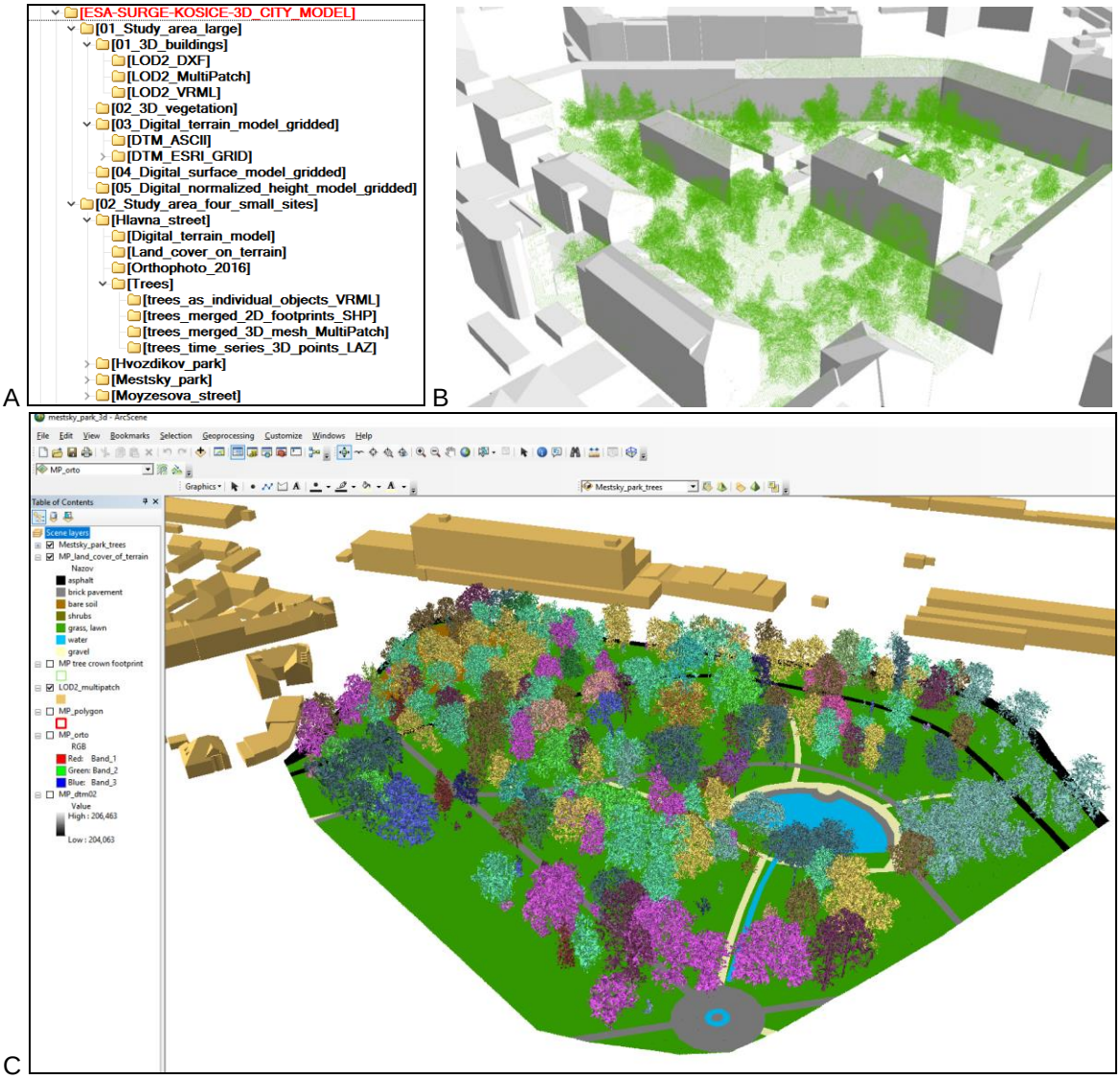


*Figure 7. Data structure of the Generated 3-D city model (Deliverable 2) (A) and detailed view of the a part of the study area (Hvozdíkov park) at LoD2 with ALS points representing trees (green) (B). Graphical interface of the ArcScene project for the small site in Mestský park (City park) showing 3D view of the geodata layers. The 3D trees are coloured according to the plant species (C).*

# 6 High-resolution urban greenery mapping for micro-climate modelling based on 3D city models.

Urban greenery has various positive micro-climate effects including mitigation of heat islands. The vegetation can stop and absorb most of incoming solar radiation mostly via the photosynthesis and evapotranspiration process. However, vegetation in mild climate of Europe, such as in Košice, Slovakia, manifests considerable annual seasonality which can also contribute to the seasonal change in the cooling effect of the vegetation on the urban climate. Modern methods of high-resolution mapping and new generations of sensors have brought opportunity to record the dynamics of urban greenery in a high resolution in spatial, spectral, and temporal domains. Therefore, we designed and applied a methodology of 3-D mapping and modelling the urban greenery during a single vegetation season of 2016. The purpose of this monitoring was to capture the change of 3-D geometry of urban greenery in ultra-high resolution and capture the effects of the change on spatial distribution of solar radiation in urban environment. Terrestrial laser scanning was conducted on four selected sites within Košice (Fig. 1). The time series of terrestrial lidar data was integrated within the 3D city model described in Section 5. This part of the SURGE study is described in Hofierka et al. (2017) and SURGE_PR2.

## 6.1 Terrestrial laser scanning

The terrestrial laser scanning (TLS) of urban greenery was performed in four study sites during the period April – November 2016 using the Riegl VZ-1000 scanner equipped with the Nikon D700 camera. The aim of the scanning was to capture vegetation in several phenological phases synchronously with the Sentinel 2A overflight times (+/- 1-2 days) taking into account meteorological conditions. TLS resulted in 44 datasets (point clouds) with total size of 93.8 GB representing the study sites in 11 time horizons during one vegetation period (Table 4). TLS required selection of appropriate positions of the scanner during the survey in order to minimize data shadows and total number of required positions. At the same time, it was important to ensure a sufficient overlap with the adjacent position (Gallay et al., 2015; Smith, 2016). Final mutual registration of individual point clouds was performed using the iterative closest point algorithm implemented as the Multi-Station Adjustment tool in the RiSCAN Pro software. The point cloud was also colourized using the digital RGB imagery acquired immediately after scanning with the integrated camera (Tab. 4, Fig. 8A). Using the Multi-Station Adjustment the standard deviation of mutual registration reached only 2 cm. Using the Multi-Station Adjustment the standard deviation of mutual registration reach only 2 cm. Achieving higher accuracy was limited by various factors such as differing accuracy of ALS and TLS or movement of tree branches induce by wind during TLS. The field survey also included geobotanical mapping when WGS84 position, plant species, basic morphological parameters and health conditions were recorded for each tree within the four smaller sites (Fig. 6). These data help to improve interpretation of the lidar point clouds and orthoimagery.

*Table 4. Dates of terrestrial laser scanning data collected on four sites in the study area of the Košice City with associated total accuracy of scans registration.*

| City park (Mestský park) | Main street (Hlavná ulica) | Moyzesova ulica (street) | Hvozdíkov park |
|---|---|---|---|

| | | | |
|---|---|---|---|
|  |  |  | 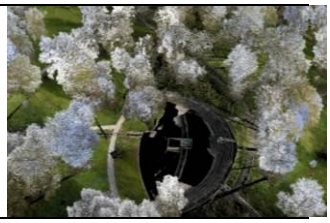 |
| April (0.032m) | April (0.029m) | April (0.062m) | April (0.045m) |
| June (0.023m) | June (0.018m) | June (0.023m) | June (0.038m) |
| July (0.029m) | July (0.014m) | July (0.023m) | July (0.016m) |
| August (0.023m) | August (0.016m) | August (0.025m) | August (0.019m) |
| September 14 (0.026m) | September 14 (0.015m) | September 14 (0.034m) | September 14 (0.018m) |
| September 23 (0.024m) | September 23 (0.016m) | September 23 (0.042m) | September 23 (0.018m) |
| October 14 (0.023m) | October 14 (0.010m) | October 14 (0.034m) | October 14 (0.017m) |
| October 27 (0.020m) | October 27 (0.010m) | October 27 (0.024m) | October 27 (0.018m) |
| November 8 (0.020m) | November 8 (0.008m) | November 8 (0.026m) | November 8 (0.017m) |
| November 23 (0.024m) | November 23 (0.012m) | November 23 (0.028m) | November 23 (0.020m) |

## 6.2 Time series of meshed 3-D tree models based on TLS

While point clouds accurately represent urban canopy, it is difficult to use this kind of geometry directly in solar radiation or microclimate models for which physical objects as virtual 3-D models are required. Therefore, we explored the following software tools to derive 3-D tree model from point clouds: RiSCAN Pro®, 3D forest, Geomagic Wrap® and ArcScene®. The result of the first step was in mutually registered and georeferenced point clouds for particular TLS survey dates. The point clouds were then decimated using the Octree filter with a spatial step of 5 cm. In this way, the georeferenced point clouds became comparable in terms of temporal change of the spatial distribution of points (Fig. 8A). Subsequent automated classification of the point clouds resulted in separating ground (terrain) and above-ground points. The above-ground points included also buildings and other features that had to be filtered out so that vegetation point remained (Fig. 8B). The mentioned procedures were performed in the RiSCAN Pro software. The point cloud representing just trees was then segmented into point clouds of individual trees by the 3D Forest software (Trochta et al., 2017). The result of segmentation was exported in the PLY format and meshed in the GeomagicWrap 2015 software to create 3-D tree models with the Wrap tool (Fig. 8C, 8D, 8F). These models were then exported in the VRML format and integrated with other 3-D data within the 3-D GIS environment of the ArcScene software (Fig. 6).

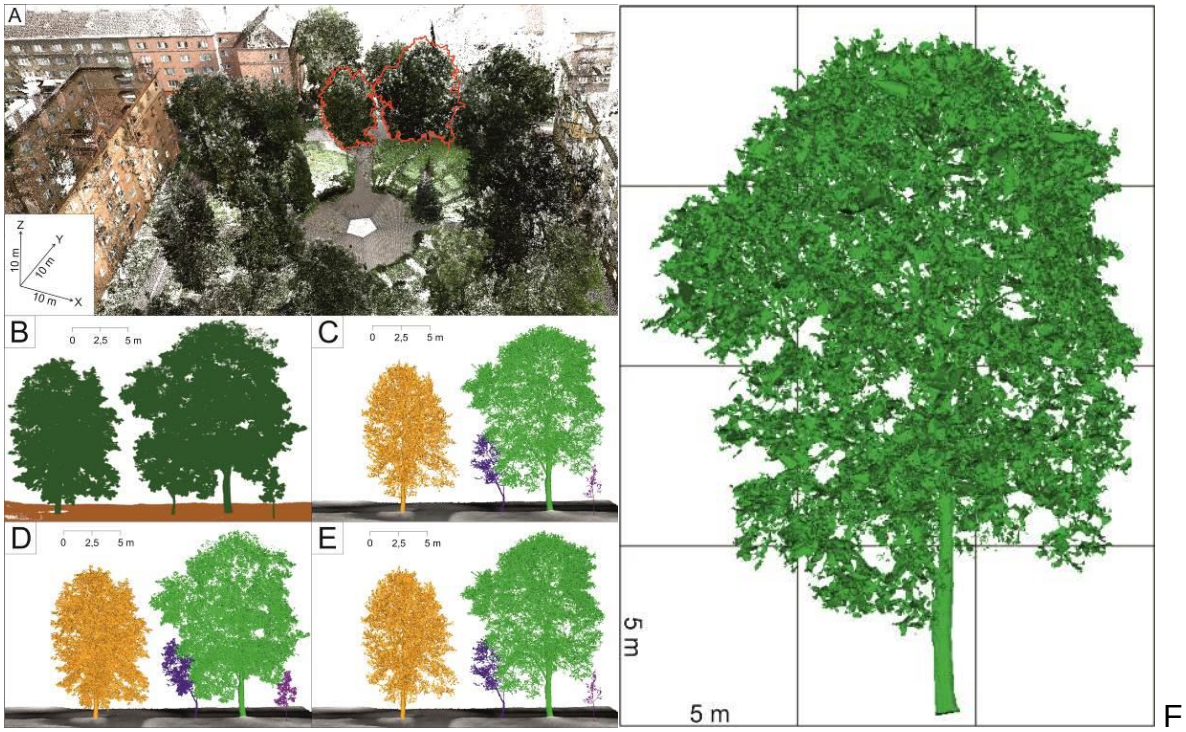


*Fig. 8. RGB colourized TLS point cloud in the RiScanPRO software with selected trees (A) which are visualized in the 3D Forest software before segmentation (B) and after segmentation and 3-D meshing in the Geomagic Wrap 2015 resulting in time series of segmented individual meshed 3-D tree models integrated with terrain data in the ArcScene GIS software for spring (C), in summer (D) and in autumn (E). Side view of the 3-D model of a tree in the GeoMagic Wrap software (F).*

## 6.3 Time series of urban greenery

Vegetation in the mild climate of Central Europe (especially broad leaved deciduous vegetation) undergoes various changes manifested mostly in tree foliage. This has also impact on solar transmissivity of the canopy and subsequently on microclimate conditions. To capture these changes throughout the vegetation period we generated time-series of point clouds acquired by TLS in four study sites. The accuracy of TLS data registration for these sites and survey days reached a standard deviation of 1-4 cm. The time-series of the scans can be found at the project web site http://esa-surge.science.upjs.sk/index.php/study-sites.

To assess the foliage of the trees in these sites we used the acquired point clouds later decimated to assess volumetric parameters of individual trees. The seasonal differences in tree morphology is demonstrated in Table 5 which reports statistics of TLS point clouds time series for a single tree growing on the Moyzesova street. We consider the mean point density and voxelized tree volume as the most significant parameters as they provide normalized values indicating that the mass of the tree decreases from the summer date through the autumn and it is the lowest in spring when there were no leaves on the tree. Implications of these results are manifested in the analysis of shaded area shown in Fig. 9. It is clear that for the selected site and time interval the effect of ground shadowing can be calculated using the generated time series of the meshed 3-D tree models. The time duration of area being shaded depends not only on the sun declination but also on the effect of the tree phenology can is involved.

*Table 5. Parameters of a single tree displayed in Fig. 6 for different dates of the TLS survey.*

| Statistics | 26 July 2016 | 27 October 2016 | 22 March 2017 |
|---|---|---|---|
| Point count | 387 500 | 389 916 | 206 631 |
| Mean density (points/m$^3$) | 4 297 | 3 146 | 2 464 |
| Total height (m) | 7.710 | 7.710 | 7.54 |
| Crown max. width (m) | 6.520 | 6.330 | 6.27 |
| Voxelized (25 cm) tree volume (m$^3$) | 99.59 | 94.25 | 81.54 |
| Footprint area (m$^2$) | 36.89 | 36.38 | 35.38 |

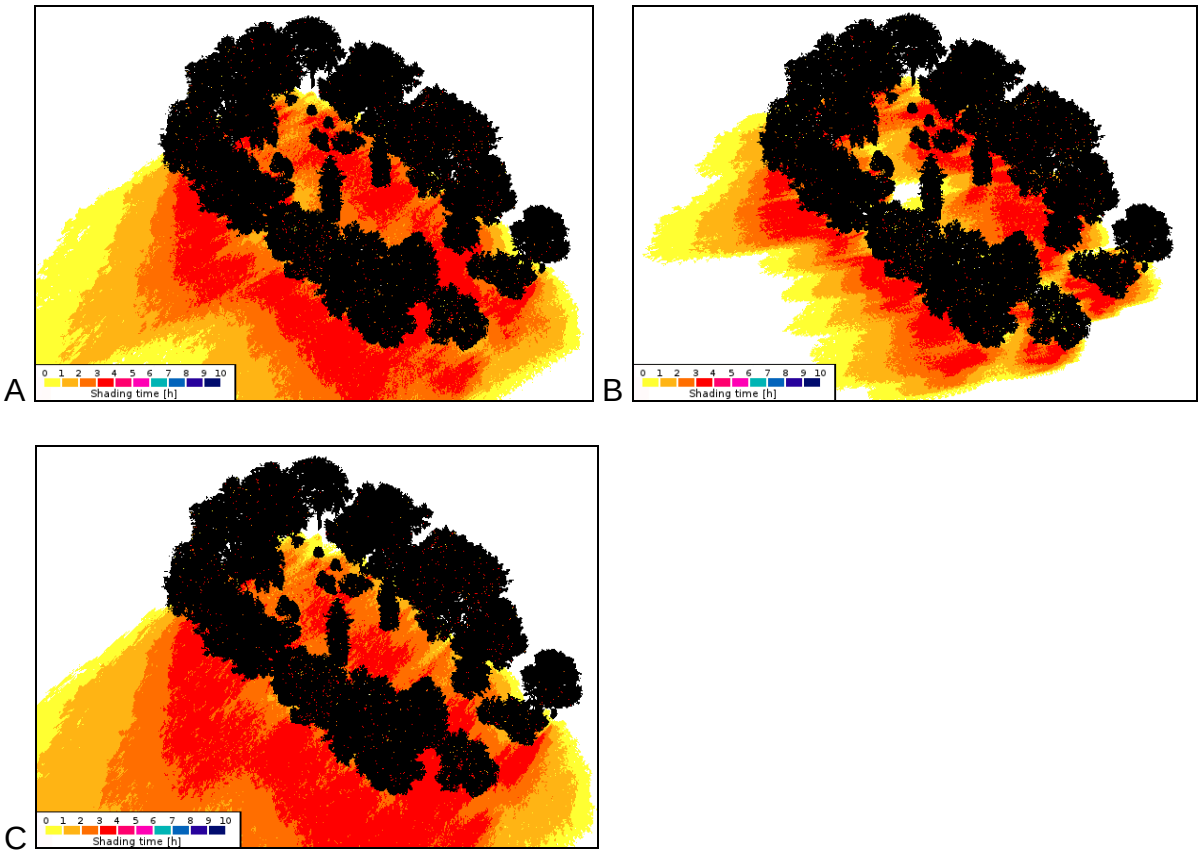


*Figure 9. Simulation of time the area is shadowed by trees between 1 p.m. to 4 p.m. using the 3-D meshed tree models in the Shadow Analysis plugin of the SketchUp software for March (A), June (B) and November (C). Adopted from Hofierka et al. (2017).*

## 6.4 Relating vegetation metrics from satellite imagery with metrics based on TLS

In modelling the solar irradiation of urban space, both atmospheric transmittance and geometric structure of urban space were shown to be critical model parameters. For the purposes of assessing the vegetation transmittance, NDVI and other indices cannot be directly used. Metrics expressing the nature of vegetation transmittance for the solar radiation comprise, for

example, leaf area index (LAI), canopy cover, tree canopy closure, canopy gap fraction, etc. However, these are difficult to be measured directly from the satellite imagery. It has been shown by many studies that, into certain extent, NDVI and other indices are correlated with the metrics and can be used as a proxy for their calculation. Tooke et al. (2012) propose that opportunities exist for incorporating additional spectral data, especially for generating estimates of the reflected component of incoming solar radiation. The potential also exists for advancing estimates of radiation transmission by articulating the temporal, spectral and structural dynamics of the local vegetation. The multispectral imagery acquired by the Sentinel 2 mission has relatively high spatial, spectral and temporal resolution to capture the dynamic of vegetation phenology. But are the properties of this data sufficient to be used as a proxy of the vegetation transmittance on higher resolution?

This question was addressed in SURGE_D4_VEGMETR 2018. This report summarised results of spatial and statistical analyses of the relationship between vegetation metrics derived from the satellite imagery of Sentinel 2 mission and the reference vegetation metrics derived from high-resolution 3-D digital representations of urban greenery. The results confirmed that Sentinel 2 multispectral imagery is strongly applicable for mapping annual phenological changes of vegetetation in urban landscape (Fig. 10). Normalized difference vegetation index (NDVI) was the most suitable metrics to parameterize the urban greenery among the tested ones (Table 6).

*Table 6. Formal definition of vegetation indices used*

| Vegetation index | Formulas |
|---|---|
| **NDVI** | (NIR-R) / (NIR+R) |
| **EVI** | 2.5 * (NIR - R) / (NIR + 6 * R - 7.5 * B + 1) |
| **EVI2** | (2.5 * (NIR – R)) / (NIR + (2.4 * R) + 1) |
| **SAVI** | (1.5 * (NIR - R) / (NIR + R + 0.5)) |

Sentinel 2: B = Band 2, R = Band 4, NIR = Band 8; Landsat 8: B = Band 2, R = Band 4, NIR = Band 5; orthoimagery: B = blue band, R = red band, NIR = near infra-red band.

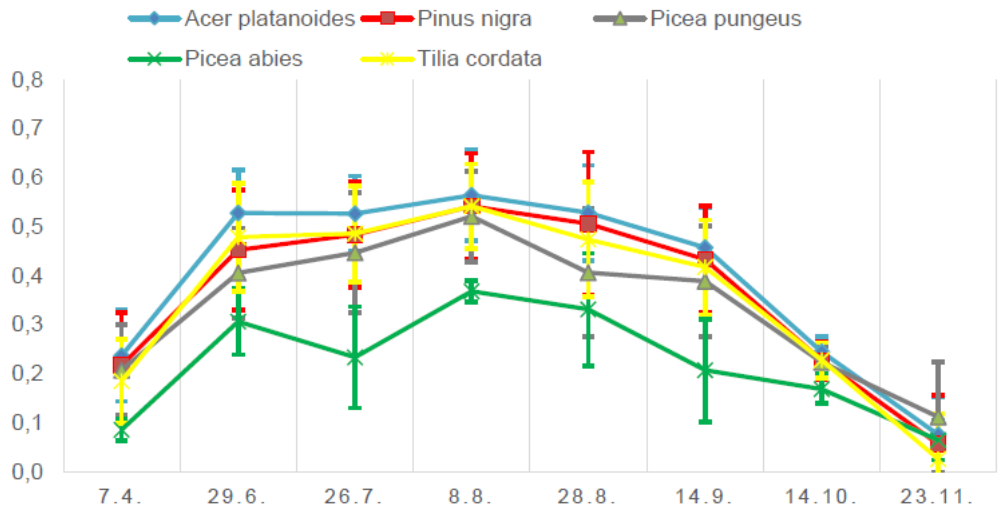


*Figure 10. Sentinel 2 based NDVI (y axis) of five most abundant tree species in Hvozdíkov park (Fig.6) throughout the year of 2016.*

Airborne (ALS) and terrestrial (TLS) laser scanning data were used to derive vegetation canopy density (CD), canopy cover (CC) and effective leaf area index ($LAI_e$). The canopy density was calculated as follows:

$$CD = Rv/A$$

Where $R_v$ is the number of vegetation lidar returns situated 1.37 m above the ground per cell area. We used 0.1 m and 10 m cell area. The canopy cover (CC) was calculated as follows:

$$CC = Ra / Rb$$

where $R_a$ is the number of lidar points situated 1.37 m above the ground, $R_b$ is the number of points below this threshold height. Recent studies have indicated the possibility to use aerial LiDAR to map $LAI_e$ in a heterogeneous urban park (Richardson et al., 2009) and in an urban environment (Alonzo et al., 2015). To estimate $LAI_e$ from ALS and TLS data, the following approach by Klingberg (2017) based on Beer-Lambert law was used:

$$LAI_e = - \beta \, . \, ln(R_{ground} / R_{total})$$

where $R_{ground}$ is the number of ground returns (including all return types), $R_{total}$ is the number of ground and canopy returns and β is a constant. β can be expected to take a value around 2, which is the theoretical value given that the foliage angle distribution is spherical and that the penetration rate of laser pulses is equal to vertical gap fraction. Richardson et al. (2009) tested four different methods to estimate $LAI_e$ from lidar data in a mixed forest in Seattle, USA and found the above described method to give the best result. The values of $LAI_e$ tend to range from 0 for bare ground to 6 for ground covered by dense vegetation. We calculated the $LAI_e$ and CC for grid cells of 10 by 10 metres to match the resolution of Sentinel 2A imagery.

Linear models (least squares regression) were applied to test for the relationship. Importantly, the NDVI derived from the Sentinel 2 imagery markedly correlated with LAIe derived from airborne and terrestrial laser scanning data (Fig. 11-14). This correlation was positive, high and stable (Pearson's r about 0.8) after development of leaves. It was weak (below 0.4) before onset of the spring bud burst and after autumn senescence. The observation provided promising outcomes for the Sentinel 2 imagery to be used as a proxy for parameterizing vegetation transmittance in solar irradiation modelling and heat flux estimation in urban space.

The findings indicated that for analysing relation of the selected vegetation metrics derived from lidar datasets and Sentinel 2A imagery NDVI correlated with more complex indices and it was decided to be sufficient for mapping the vegetation by Sentinel 2A. Canopy cover and canopy density derived from TLS and ALS data had weak correlation with NDVI derived from Sentinel 2A data. High NDVI values of Sentinel 2 imagery were co-located with high values of canopy density and canopy cover and vice versa. LAIe based on TLS and ALS most closely correlated with NDVI derived from Sentinel 2A data. This correlation was strong in the vegetation season and lower off this season. However, such relationship was not observed on all TLS sites and if the data from sites are merged together per date the relationship is weak (Fig. 15). The results opened more issues and questions to address than were answered. One of the most important is whether and how the response of the defined linear models can be improved and if a more suitable set of vegetation metric can be identified for relating the information of Sentinel 2 with 3D geometry. The lessons learned suggest that more robust statistical models are needed to find closer fit beteween Sentinel 2 NDVI and TLS derived metrics for downscaling the vegetation transmittance to higher resolutions. The reliability of the prediction of the vegetation transmittance from the Sentinel 2 data based on the reported findings requires further testing.

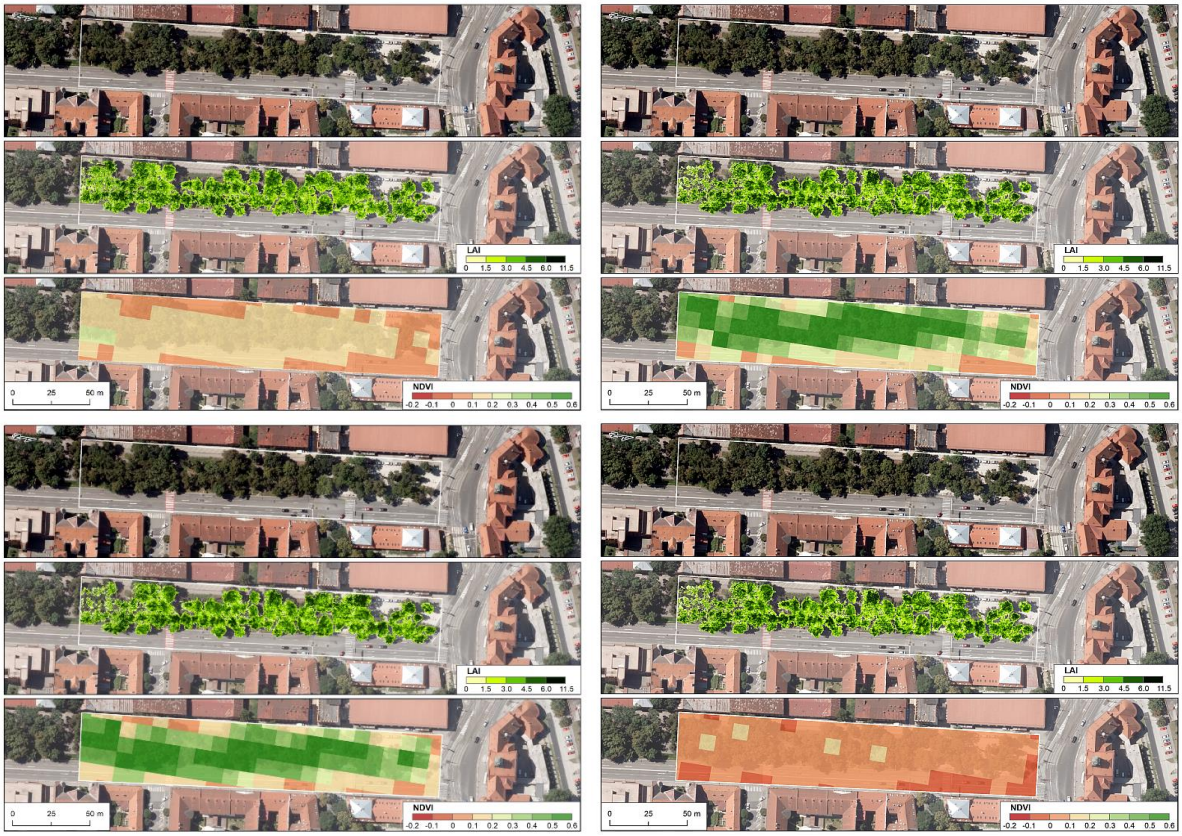


*Figure 11. $LAI_e$ per 0.1 m cell size from TLS data and Sentinel 2A NDVI for 10 m cell size for the site of Moyzesova street. Data acquisition: 7 April 2016 (top left), 26 July 2016 (top right), 27 August 2016 (bottom right), 23 November 2016 (bottom right).*

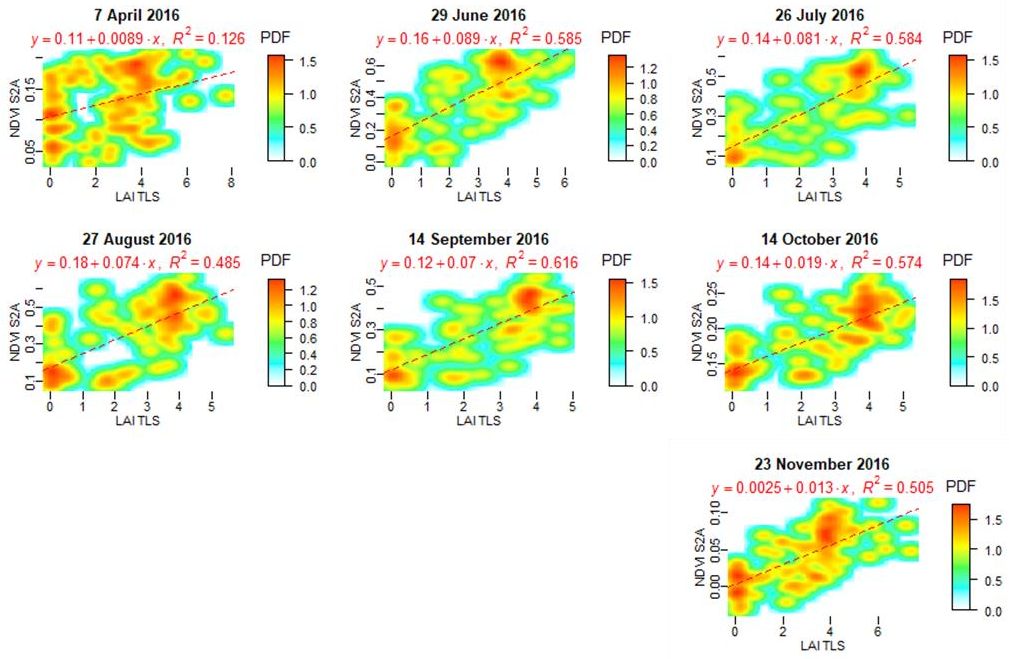


*Figure 12. Smoothed scatterplots of Sentinel 2A NDVI and $LAI_e$ canopy density calculated at 0.1 m grid cell size for the site of Moyzesova street.*

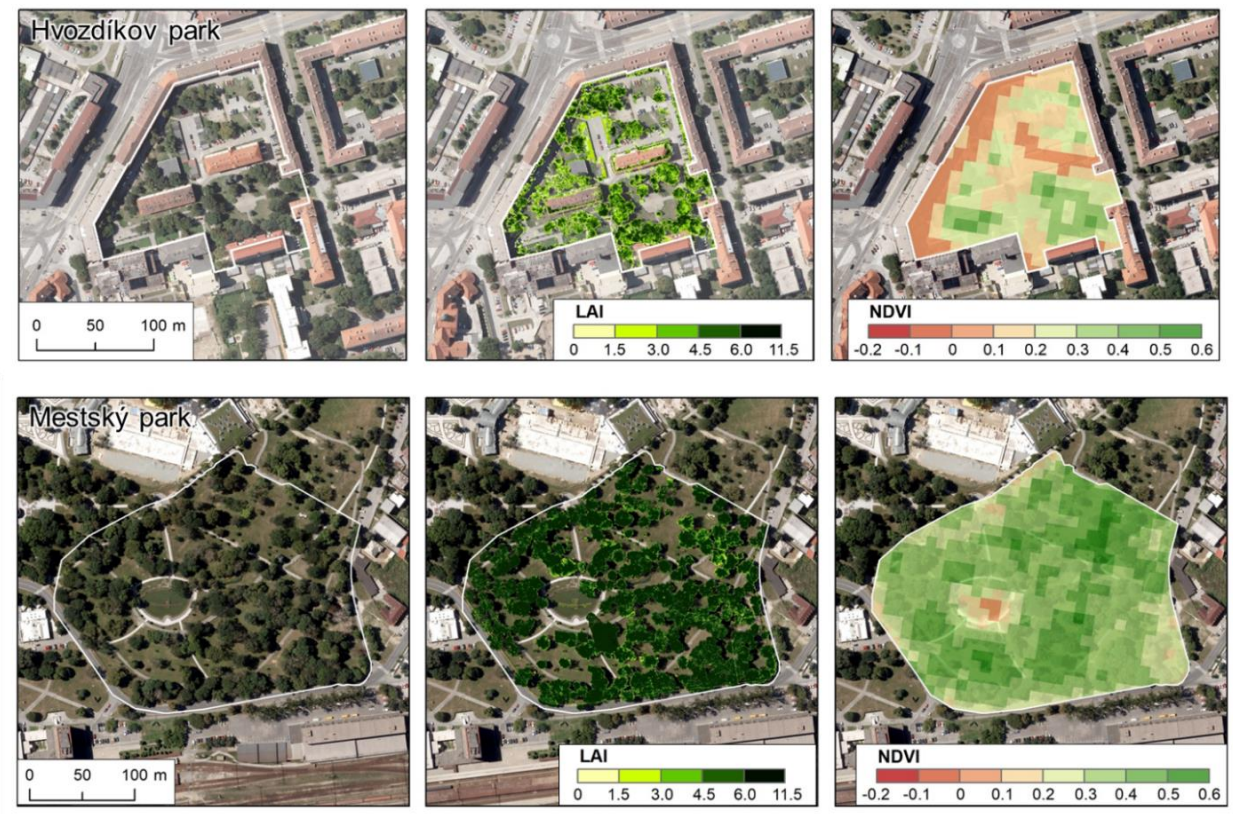


*Figure 13. $LAI_e$ per 0.1 m cell size from TLS data and Sentinel 2A NDVI for 10 m cell size for the site of Hvozdíkov park and Mestský park. Data acquisition: 27 August 2016.*

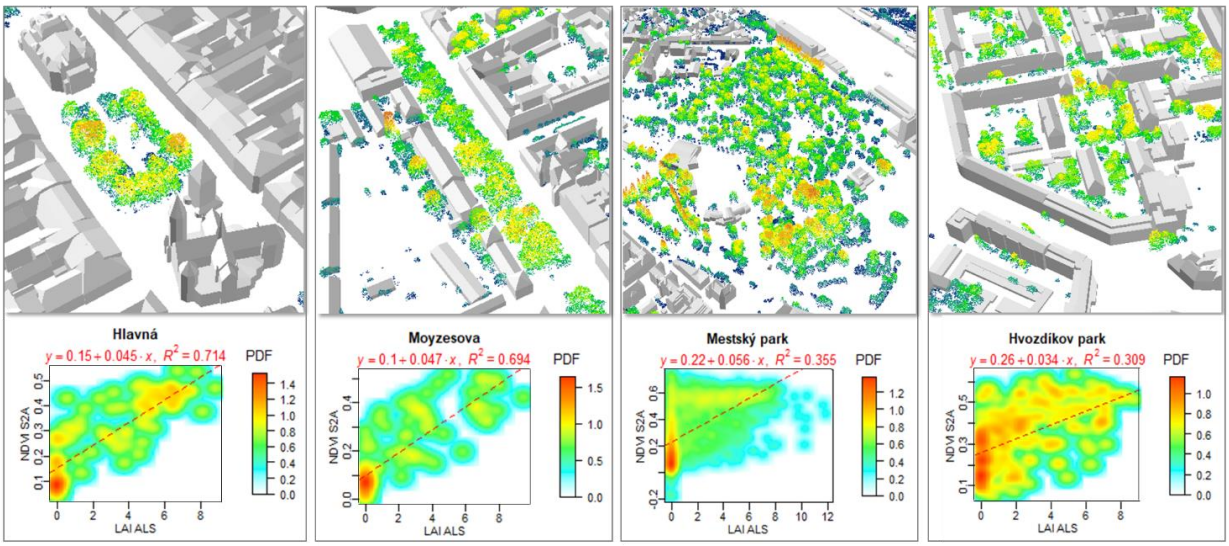


*Figure 14. $LAI_e$ per 10 m cell size from ALS data and Sentinel 2A NDVI for 10 m cell size for all four small sites. Data acquisition: 14 September 2016.*

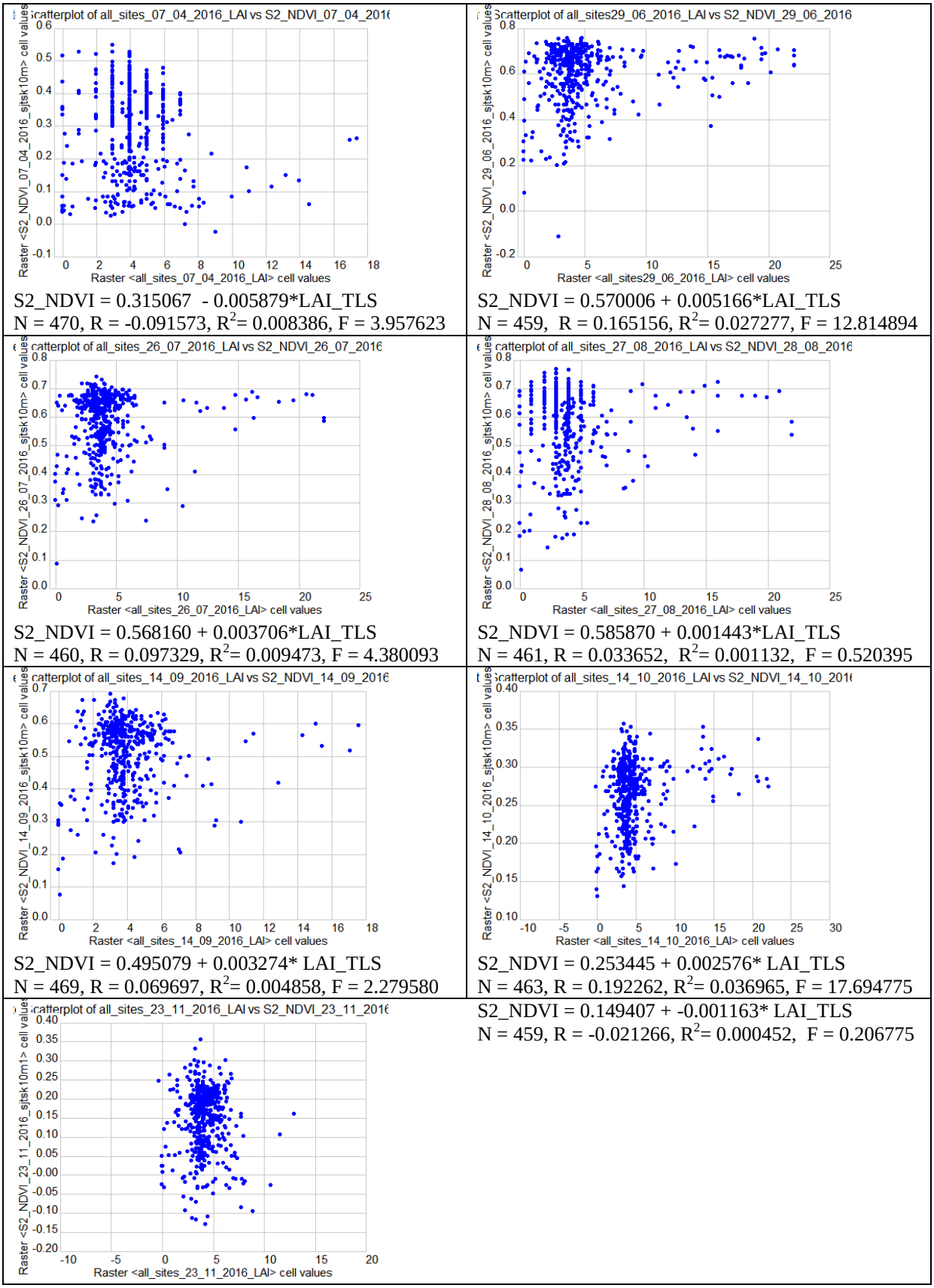


*Figure 15. Scatter plots and liner regression models with statistics for estimated leaf area index derived from TLS time series and NDVI derived from Sentinel 2 imagery, both parameters are calculated for 10 m spatial resolution for all 4 sites merged together.*

# 7 Novel algorithmic structure for spatial modelling of land surface temperature and simulating the cooling effect of vegetation

Mitigation of urban heat islands (UHI) requires understanding of the factors affecting the interaction of solar radiation and urban surfaces. Over the last two decades numerous studies have been published analysing the associations between solar radiation, reflectance, emissivity and other heat transfer parameters of materials of urban surfaces (Berdahl and Bretz, 1997, Mirsadeghi et al. 2013). Land Surface Temperature (LST) is considered to be a reliable indicator of the UHI as there is a close correlation between the LST and near-surface air temperature due to transfer of thermal energy emitted from the surface to the atmosphere (Nichol, 1994). However, due to the fact that air mixes within the atmosphere, the relationship between surface and near-surface air temperatures is not constant and changes during the day and night (EPA, 2008). LST is generally defined as the radiative skin temperature of the ground. LST is a key parameter in the physics of land surface processes, combining surface-atmosphere interactions and energy fluxes between the atmosphere and the ground. Properties of urban materials, in particular solar reflectance, thermal emissivity, and heat capacity influence the LST and subsequently development of UHIs, as they determine how the Sun's energy is reflected, emitted, and absorbed. The SURGE_D5_ALGOSTRUC report comprises details on the design of the algorithm, i.e. workflow, of how we approached the modelling of the cooling effect of urban greenery taking into account the information extracted from the S2 mutlispectral imagery.

## 7.1 Spatial modelling of solar irradiation

Solar radiation received at the urban surface is a key input factor in many urban energy models and sustainable city designs. Examples include thermal and photovoltaic solar energy installations, passive heating systems or urban microclimate designs. However, solar radiation flows over urban surfaces are highly variable due to a complexity of urban morphology and interactions with various components of the urban environment. The use of adequate models and tools is therefore crucial for accurate assessments of spatial and temporal distribution of solar radiation in urban areas. Over the last two decades several solar radiation models integrated with geographical information systems (GIS) were developed. These GIS-based solar radiation models provide estimates of spatial variations of solar radiation over large regions using digital terrain models (DTMs) and selected ground-based or satellite data reflecting atmospheric and land cover conditions (e.g., Dubayah and Rich 1995, Šúri and Hofierka 2004). These solar radiation models can be used for two-dimensional (2-D) surfaces, such as land surface or rooftops. Hofierka and Zlocha (2012) also developed the v.sun model as a full 3-D solar radiation model for complex, three-dimensional (3-D) urban surfaces as an extension of the r.sun model.

The original proposal in this feasibility study was to simulate the cooling effect of urban greenery using the Sentinel 2 data with the v.sun module. However, we realised that Sentinel 2 data could be implemented into such a geospatial modelling in a simpler fashion via the r.sun module which will be more convenient for the end user. The main argument for that is the two-dimensionality of Sentinel 2 data products which represent a 2D array of spectral radiance reflected from the earth surface and recorded by the MSI sensor on-board the

satellite vehicle. The data products are 2D arrays by nature, i.e. raster datasets, therefore, more suitable for the r.sun module which was developed for 2D raster data.

The r.sun model is implemented in the open-source environment of GRASS GIS as the r.sun module (Neteler and Mitasova 2004) and it is one of the widely used GIS-based solar radiation models. Originally developed as a clear-sky model (Hofierka 197), it was later further substantially improved by Šúri and Hofierka (2004) to include diffuse and reflected components of solar radiation for clear-sky and real-sky conditions. The model is sufficiently robust and flexible over various scales and range of applications.

Table 7 summarizes computation of the global solar irradiance in GRASS GIS for 4 scenarios for the 182th day of year and 10:20 of zonal time (30 June 2016). This day and time was selected for the availability of cloudless scenes of Landsat 8 for this moment and Sentinel 2 for previous day of 29 June 2016. The scenarios demonstrate the effect of urban greenery on the temperature of the land surface. Trees and shrubs taller than 1.5 m are considered for simulating this effect.

*Table 7. Different scenarios of input parameters for modelling the global solar irradiance and the effect of urban greenery.*

| **Modelled scenario** | **Variable input parameters** |
|---|---|
| 1 | • Surface of the ground/terrain and buildings, and its slope angle and slope aspect<br>• Surface broad-band albedo (albedo, 0-1) derived from Sentinel 2 for 29 June 2018 (day of year 181, 10:40 zonal time)<br>• No transmittance of urban greenery, irradiation modelled for the canopy surface of urban greenery<br>`r.sun --o elevation=DSM_ground+buildings aspect=DSM_ground+buildings_aspect slope=DSM_ground+buildings_slope albedo=albedo_182 beam_rad=b182i1020 diff_rad=d182i1020 refl_rad=r182i1020 day=182 time=10.33`<br>`r.mapcalc "g182i1020 = b182i1020 + d182i1020 + r182i1020"` |
| 2 | • Surface of the ground/terrain and buildings,<br>• Surface broad-band albedo (albedo, 0-1) derived from Sentinel 2 for 29 June 2018 (day of year 181, 10:40 zonal time)<br>• Variable transmittance of urban greenery (coeff_bh, 0-1), estimated with linear regression models of LAI_TLS and S2_NDVI for site 1<br>`r.sun --o elevation=DSM_ground_buildings_vegetation aspect=DSM_ground_buildins_vegetation_aspect slope=DSM_ground_buildins_vegetation_slope albedo=albedo_182 beam_rad=bveg182i1020r diff_rad=dveg182i1020r refl_rad=rveg182i1020r day=182 time=10.33 coeff_bh=real_coeff20160914`<br>`r.mapcalc "gveg182i1020r = bveg182i1020r + dveg182i1020r + rveg182i1020r"` |
| 3 | • Surface of the ground/terrain and buildings and urban greenery, and its slope angle and slope aspect<br>• Surface broad-band albedo (albedo, 0-1) derived from Sentinel 2 for 29 June 2018 (day of year 181, 10:40 zonal time)<br>• No transmittance of urban greenery, irradiation modelled for the canopy surface of urban greenery<br>`r.sun --o elevation=DSM_ground_buildings_vegetation aspect=DSM_ground_buildins_vegetation_aspect slope=DSM_ground_buildins_vegetation_slope albedo=albedo_182 beam_rad=bveg182i1020 diff_rad=dveg182i1020 refl_rad=rveg182i1020 day=182 time=10.33`<br>`r.mapcalc "gveg182i1020 = bveg182i1020 + dveg182i1020 + rveg182i1020"` |
| 4 | • Surface of the ground/terrain and buildings and urban greenery, and its slope angle and slope aspect<br>• Surface broad-band albedo (albedo, 0-1) derived from Sentinel 2 for 29 June 2018 (day of year 181, 10:40 zonal time)<br>• Variable transmittance of urban greenery (coeff_bh, 0-1), estimated with linear regression models of LAI_TLS and S2_NDVI for site 1<br>`r.sun --o elevation=DSM_ground+buildings aspect=DSM_ground+buildings_aspect slope=DSM_ground+buildings_slope albedo=albedo_182 beam_rad=b182i1020r diff_rad=d182i1020r refl_rad=r182i1020r day=182 time=10.33 coeff_bh=real_coeff20160914`<br>`r.mapcalc "g182i1020r = b182i1020r + d182i1020r + r182i1020r"` |

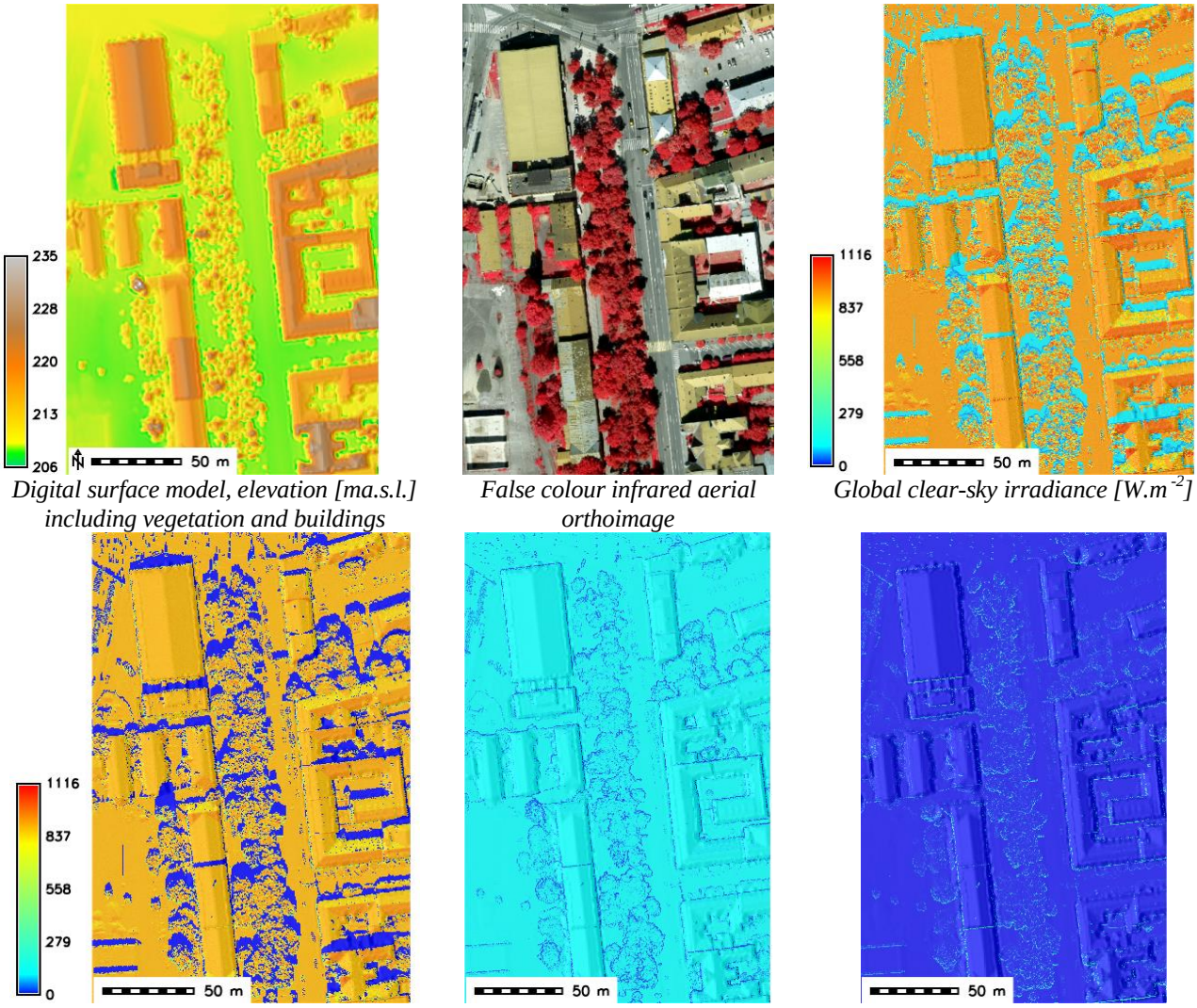


*Digital surface model, elevation [ma.s.l.] including vegetation and buildings*

*False colour infrared aerial orthoimage*

*Global clear-sky irradiance [W.m$^{-2}$]*

*Beam (direct) irradiance [W.m$^{-2}$]*

*Diffuse irradiance [W.m$^{-2}$]*

*Reflected irradiance [W.m$^{-2}$]*

*Figure 16. Lidar based digital surface model (DSM) of the area of Moyzesova street in Košice (site 1 in Fig. 1) including buildings and vegetation used to calculate global solar irradiance (W.m$^{-2}$) with its components using the r.sun model in GRASS GIS for 30 June at 10:20 zonal time. The area size is 200 m by 400 m. The resulting data layers were derived at 0.50 m spatial resolution.*

Grass, lawns and small shrubs are considered as land cover of the ground surface. The calculated global solar irradiance on horizontal surfaces such as roads (orange colour of global irradiance in Fig. 16) corresponds well with the measured global irradiance at the Košice airport weather station on (887.15 W.m$^{-2}$) on 30 June 2016 at 10:00 zonal time. The final output of each of the four scenarios resulted in a sum of the beam, diffuse and reflected component which is the global irradiance raster layer. This dataset is one of the key inputs for modelling the temperature which is described in the following section.

## 7.2 Spatial modelling of land surface temperature

The land surface temperature was estimated by a novel algorithm combining map algebra in GRASS GIS, the Stefan Boltzmann Law and the Kirchhoff rule using raster input data

derived from a virtual 3D city model and Sentinel 2 multispectral imagery. Generally, a built-up area exhibits a variable thermal pattern with hot and cold peaks, corresponding to low and high reflectivity impervious surfaces, respectively. A solar-reflective surface is typically light in colour and absorbs less sunlight than a conventional dark-coloured surface. Mitigating UHIs requires lowering the average surface temperature of the city so that there is less surface-to-air heat transfer. Urban vegetation is one of key components of this effort as the greenery maintains cooler surface temperatures, mainly by the process of evapotranspiration and shading. For building and pavement surfaces in the sun, surface characteristics such as albedo, emissivity, and roughness, are also relevant. For a surface under the sun and insulated underneath, the equilibrium surface temperature, *Ts* is obtained from the equation based on Stefan-Boltzmann Law which describes the power radiated from a black body in terms of its temperature (Bretz et al., 1998):

$$(1-\alpha)I = \varepsilon\sigma\left(T_s^4 - T_{sky}^4\right) + h_c\left(T_s - T_a\right) \qquad \text{Eq. 1}$$

where $\alpha$ is unitless solar-reflectivity or albedo of the surface varying from 0 to 1, $I$ is the total solar radiation incident on the surface in W.m$^{-2}$ which is the output from the r.sun model, $\varepsilon$ is the emissivity of surface, $\sigma$ is the Stefan-Boltzmann constant, $5.6685 \times 10^{-8}$ W.m$^{-2}$K$^{-4}$, $T_s$ is equilibrium surface temperature, K, $T_{sky}$ is the effective radiant sky temperature, $h_c$ convection heat transfer coefficient, Wm$^{-2}$K$^{-1}$, $T_a$ air temperature, K (ASHRAE, 1989).

Using this equation, the surface temperature $T_s$ can be approximated by Newton's iteration method. In GRASS GIS using a shell script this approximation has the following form:

```
#!/bin/sh
#lst.stefan-boltzman.sh
echo "Global irradiance file"
read irr
g.copy rast=$irr,gi
echo "Albedo file"
read alb
g.copy rast=$alb,albedo
echo "Convection coefficient file"
read cc
g.copy rast=$cc,h_c
echo "Initial estimation of land surface temperature (e.g., 300)"
read temp0
echo "Ambient air temperature (e.g., 293)"
read T_a
echo "Radiant sky temperature (e.g., 287)"
read T_sky
echo " initialization of parameters..."

r.mapcalc --o "epsilon = 1. - albedo"
r.mapcalc --o "c = -epsilon * 0.000000056685 * $T_sky * $T_sky * $T_sky *
$T_sky - h_c * $T_a - (1 - albedo) * gi"

r.mapcalc --o "lst0 = $temp0" #initialization of LST
r.mapcalc --o "y = lst0*lst0*lst0"
r.mapcalc --o "lst = (3*epsilon*0.000000056685*y*lst0 -
c)/(4*epsilon*0.000000056685*y+h_c)" #1st iteration

  i=2
  while  [ $i -le 10 ]
  do
```

```
  echo "Iteration" $i

g.copy --o rast=lst,lst0
r.mapcalc --o "y = lst0*lst0*lst0"
r.mapcalc --o "lst = (3*epsilon*0.000000056685*y*lst0 -
c)/(4*epsilon*0.000000056685*y+h_c)"
   i=`expr $i + 1`
 done
echo "Finished."
```

This approximation requires the first estimation of LST (e.g., roughly close to measured air temperature, sunny, overcast day, etc.). Then 10 iterations produce the results with sufficient accuracy. The GRASS GIS implementation assumes that ambient air temperature $T_a$ and radiant sky temperature $T_{sky}$ are also known. Air temperature is usually measured by meteorological stations, often even within the city. Radiant sky temperature can be estimated using one of the available approximation methods published, e.g. in (Algarni, 2015), depending on the cloudiness. In this study, we use fairly simple clear sky and cloudy sky direct temperature models where $T_{sky} = T_a - 20$ under clear-sky conditions (Garg, 1982) and $T_{sky} = T_a - 6$ under cloudy conditions (Whillier, 1967). Of course, any other temperature model can be used depending on available data to improve the accuracy of assessment. However, to evaluate the algorithmic structure of our solution it is sufficient to use even these simple formulas. The dominant parameters which determine the maximum LST are solar reflectance (albedo) $\alpha$, thermal emissivity of the surface $\varepsilon$ and convection heat transfer coefficient $h_c$. Berdahl and Bretz (1997) demonstrated a fairly linear correlation between albedo and thermal emissivity of the surface for typical metal roof coatings and in most cases emissivity can be roughly approximated by $(1-\alpha)$.

The relationship between albedo and thermal emissivity is generally called Kirchoff's Law saying that surfaces with high reflectivity (or, roughly, high albedo) have low emissivity and vice versa. Based on this law, we assume for an arbitrary body emitting and absorbing thermal radiation in thermodynamic equilibrium, the emissivity is equal to the absorptivity of the incomming electromagnetic energy.

$$absorption = emissivity\ at\ a\ specific\ wavelength$$

$$(1 - albedo) = emissivity$$

Despite it is known that this assumption does not rigidly hold it can be used for approximating the emissivity in case other more accurate data do not exist. Moreover, emissivity can be calculated from Sentinel 2 data by deriving broad-band albedo as described in Section 7.3.

The convection coefficient $h_c$ is usually the most difficult parameter to estimate. It depends strongly on wind speed and direction, geometry of the building and surroundings objects, height of the roof above ground level, building material texture (roughness) and surface to air temperature difference (Mirsadeghi et al., 2013).

In sunlight, with zero wind speed, $h_c$, is determined by natural convection. It is a weakly increasing function of temperature difference, and almost independent of surface size. For example, for $T_{sky} - T_a = 30$ K, estimates give $h_c = 6.6$ $Wm^{-2}K^{-1}$. For wind speeds above 1 $m.s^{-1}$, the convection coefficient is determined by forced convection, and, $h_c$ rises from 2.5 to 3.0 $W.m^{-2}.K^{-1}$ at zero wind speed to about 15 to 20 $W.m^{-2}.K^{-1}$ at wind speeds of 7 $m.s^{-1}$ with even higher values of $h_c$ for roofs and upwind surfaces (Liu et al., 2015). More accurate estimates of $h_c$ require complex modelling techniques using 3D city models, data on building material and

3D wind simulation. In this study, we use a uniform value of $h_c$ =10 W.m$^{-2}$.K$^{-1}$ for the whole study area but also spatially differentiated $h_c$ based on land cover type to account for spatial differences within the city or between the buildings. Table 8 summarizes how we assigned different land cover categories with the values of $h_c$ which was based on expert judgment supported by the values reported by Liu et al. (2015), Vollaro et al., (2015) and Amir et al. (2018). The values are estimated for typical hot summer atmospheric conditions with clear sky, small or no wind. The resulting LST was calculated for four scenarios using the detail of the study area of site 1 as Figure 17 and 18 demonstrate. These figures also show the cooling effect of urban trees and shurbs.

*Table 8. Convective heat transfer coefficient used in this study for modelling the surface temperature in the Košice city*

| **Surface material** | **Convective heat transfer coefficient [W.m$^{-2}$.K$^{-1}$]** |
|---|---|
| roofs | 8 |
| dark grey and dark pink asphalt roads and pavements, red bricks, concrete, concrete paver blocks, concrete paver blocks with tram rails, crushed stone pavement, dark stone blocks pavement, loose pebbles pavement, gravel stones, red clay courts, railway, stone graves with grass | 10 |
| concrete channel with water | 12 |
| bare soil | 13 |
| grass, lawn, low shrubs | 15 |
| low shrubs | 15 |
| water surface | 20 |

This $h_c$ parameter is important in modelling the global solar irradiance and in approximating the surface emissivity. The use of Sentinel 2 data in ascertaining the solar vegetation transmittance is a more complex task. In the study, the relationship between NDVI and LAI_TLS for corresponding dates was found to be weak and insignificant, thus unreliable for downscaling the solar vegetation transmittance.

We recognize that the heat transfer is a complex phenomenon and therefore it is difficult to ascertain realistic values of the input parameters of the proposed approach of converting solar irradiance to land surface temperature. Nevertheless, the algorithm provides means for assessing various scenarios in urban planning for mitigating urban heat island or summer heat waves in general. Most importantly, the outlined approach enables to model the surface temperature on a much finer scale than it is sensed by contemporary thermal sensors such as TIRS of Landsat 8 or SLSTR of Sentinel 3. Both sensors record the LST phenomenon on a different and broader spatial scale than was modelled by the proposed algorithm. The two kinds of LST data products are therefore difficult to compare for the modifiable area unit problem (MAUP) which his demonstrated by Figure 19. Atmospherically corrected LST was derived from a Landsat 8 scene acquired on 30 June 2016 10:20 zonal time using the approach presented in Onačillová & Gallay (2018). The LST was modelled by the algorithm for the same date and time for comparison at spatial resolution of 30 metres for the comparison with Landsat 8 LST. The general patterns can be recognized in both datasets which is expressed also by the distribution of the LST values in the scatterplot showing linear relationship. However, the LST modelled with our approach is heavily overestimated in areas which are generally hot associated with railway station and continuous built-up areas while they are only several degrees underestimated in areas where urban greenery is present. The modelled LST requires further validation with more realistic records of the temperature, for example, airborne thermal

data. Nevertheless, a good match with the L8 LST supports the viability of the developed approach of LST modelling.

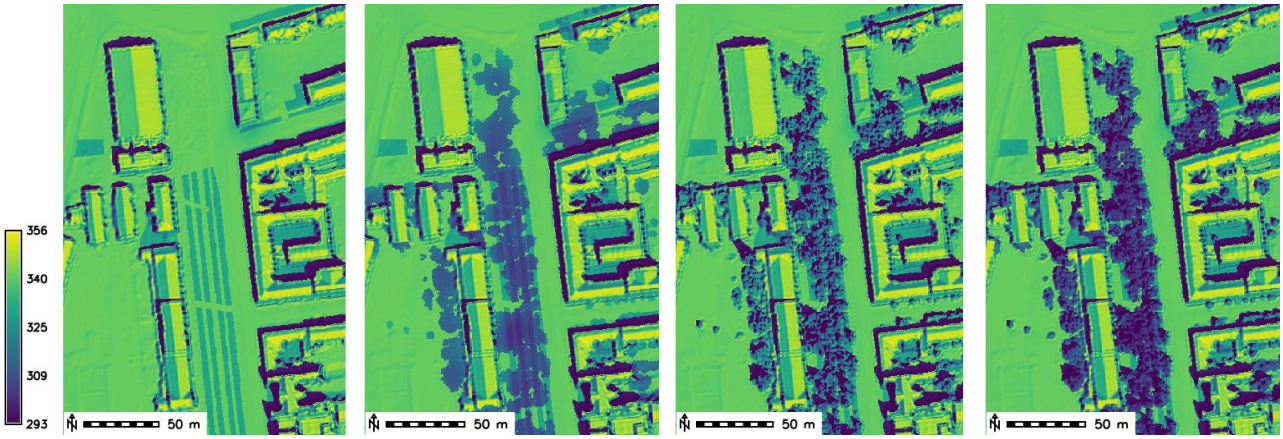


DSM with buildings, Albedo of ground land cover, No trees
`lst182i1020`

DSM with buildings, Albedo of ground land cover, Solar transmittance of trees
`lst182i1020r`

DSM with buildings and trees, Albedo of land cover
`lstveg182i1020`

DSM with buildings and trees, Albedo of land cover Solar transmittance of trees
`lstveg182i1020r`

*Figure 17. Modelled temperature of ground surface (kelvins) in site 1 - Moyzesova street, without and with implementing vegetation transmittance downscaled from linear regression model os S2_NDVI vs. LAI_TLS for 30 June 2016 at 9:20 AM of UTC, 10:20 zonal time. In the first two images DSM of terrain and building surface is used and albedo is derived for the ground land cover below the trees. In the latter two images, DSM of terrain, buildings and trees is used and albedo of the land cover canopy surface was used.*

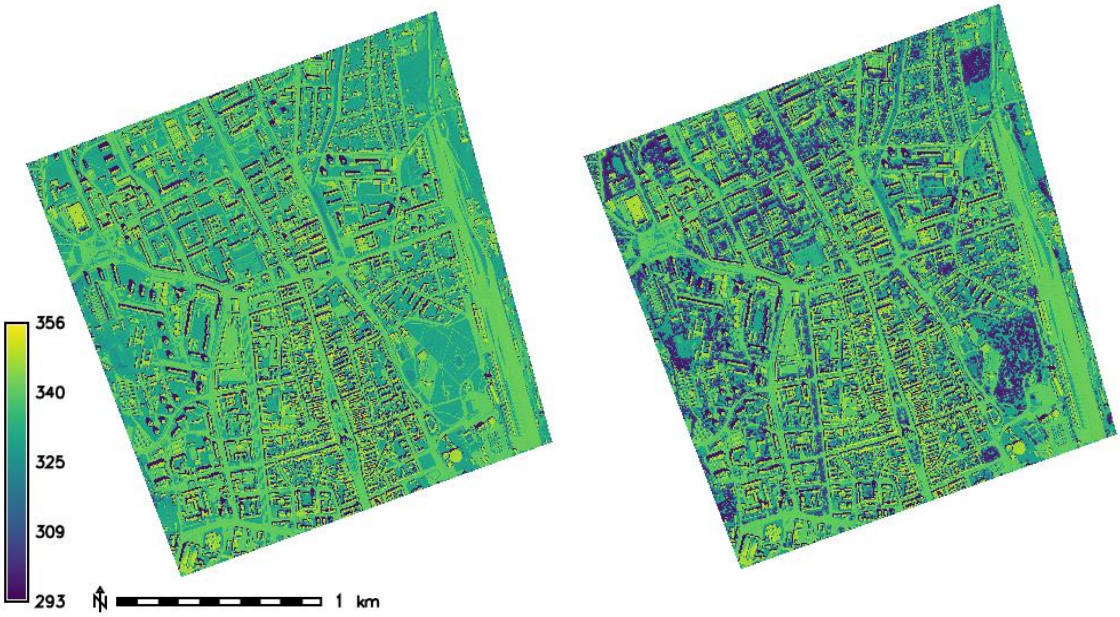


DSM with buildings, Albedo of ground land cover, No trees
`lst182i1020`

DSM with buildings, Albedo of ground land cover, Solar transmittance of trees
`lstveg182i1020r`

*Figure 18. Modelled temperature of ground surface (kelvins) in the entire study area of Košice without and with implementing vegetation transmittance downscaled from linear regression model os S2_NDVI vs. LAI_TLS for 30 June 2016 at 9:20 AM of UTC, 10:20 zonal time.*

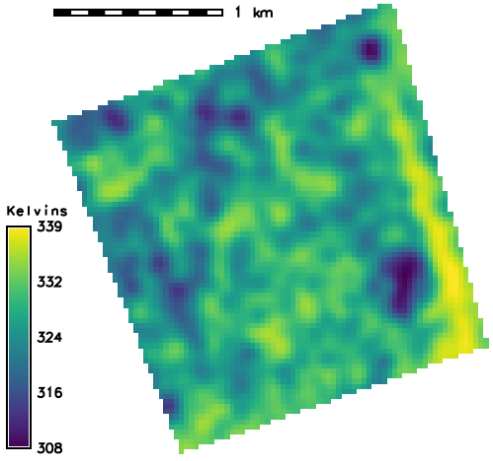


Modelled temperature with main inputs:
DSM with buildings and trees,
Albedo of land cover (including trees)
Calculated at 30 m cell size.

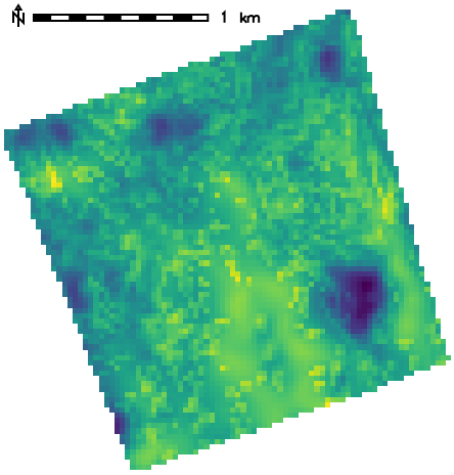


Landsat 8 land surface temperature at the bottom of the atmosphere

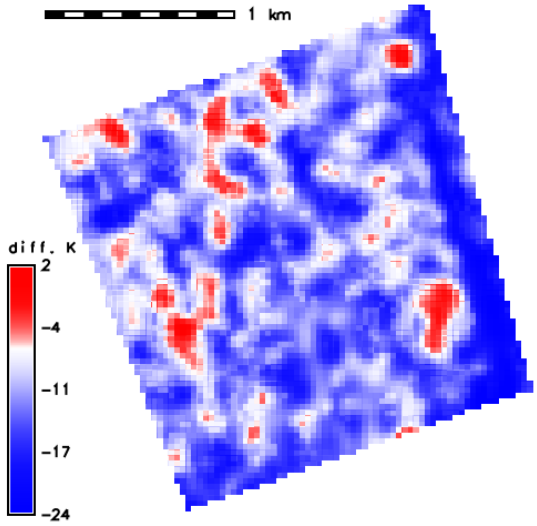


Differences between the Landsat8 observed and modelled temperature in degrees Kelvin

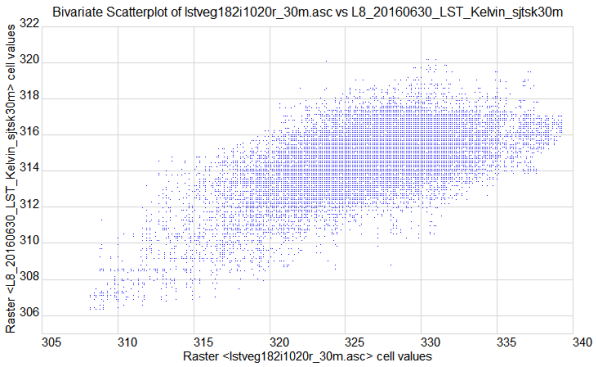


Scatterplot of modelled temperature and temperature sensed by Landsat 8 TIRS Band 11 at 30 m spatial resolution

*Figure 19. Modelled temperature of land cover surface (left) derived for 30 June 2016 at 9:20 AM of GMT 10:20 zonal time and land surface temperature at the bottom of the atmosphere (right) as sensed at the same time by Landsat 8 TIRS, band 11. The spatial resolution (raster cell size) is 30 m, the units of temperature are degrees Kelvin.*

## 7.3 The role of Sentinel 2 in LST calculation

Sentinel 2 mission provides multispectral imagery in visible and infrared spectrum at spatial resolutions of 10, 20, and 60 metres. The spectral range approximately covers the wavelengths from 440 nm to 2,200 nm. Thus, no direct means of thermal sensing is possible with Sentinel 2

sensors. However, several data types can be derived from the Sentinel 2 imagery which can be used in the proposed algorithm of LST calculation. We experimented with the surface albedo and NDVI parameters for deriving input raster layers for the LST calculation. Given the temporal resolution of the Sentinel 2 mission, such data products can be provided and updated every 5 days. The first useful parameter is, ***the broad-band surface albedo*** which was calculated as the integration of at-surface reflectance across the shortwave spectrum (D'Urso and Calera, 2006):

$$\alpha = \sum_{bi}^{n} |\rho_{bi} * \omega_{bi}|$$

where $\alpha$ is albedo, $\rho_{bi}$ is surface reflectance for a given band *bi* at Level-2A Sentinel-2A surface reflectance, obtained using the ESA's Sen2Cor algorithm (Version 2.3.1), $\omega_{bi}$ is the weighting coefficient representing the solar radiation fraction derived from the solar irradiance spectrum (Thuillier et al., 2003) within the spectral range (spectral response curves) for bands *bi* as indicated with *Esun* in Table 9. This approach of surface albedo calculation was applied by Vanino et al. (2018) in the study of evapotranspiration and irrigation requirements for tomato crop in Central Italy. The Sen2Cor algorithm (Müller-Wilm, n.d) processes S2 Level 1C data to an orthoimage bottom-of-atmosphere (BoA) corrected reflectance product (Level 2A). The algorithm is available within the Sentinel Application Platform (SNAP), which is a software package tailored to the Sentinel-2 characteristics, developed by ESA (http://step.esa.int/main/toolboxes/sentinel-2-toolbox/sentinel-2-toolbox-features/ ). The SNAP is provided free of charge and other added value products such as various land cover indices or biophysical biophysical products can be derived from Sentinel-2 reflectance data.

*Table 9. Weighting coefficients for the calculation of broad-band albedo from Sentinel 2 data.*

| **Band Number** | **Spatial resolution (m)** | **Center λ (µm)** | **Spectral width Δλ (µm)** | **Esun (W m$^{-2}$)** | $\omega_{bi}$ |
|---|---|---|---|---|---|
| **1** | 60 | 0.443 | 0.020 | 1893 | |
| **2** | 10 | 0.490 | 0.065 | 1927 | 0.1324 |
| **3** | 10 | 0.560 | 0.035 | 1846 | 0.1269 |
| **4** | 10 | 0.665 | 0.030 | 1528 | 0.1051 |
| **5** | 20 | 0.705 | 0.015 | 1413 | 0.0971 |
| **6** | 20 | 0.740 | 0.015 | 1294 | 0.0890 |
| **7** | 20 | 0.783 | 0.020 | 1190 | 0.0818 |
| **8** | 10 | 0.842 | 0.115 | 1050 | 0.0722 |
| **8a** | 20 | 0.865 | 0.020 | 970 | |
| **9** | 60 | 0.945 | 0.020 | 831 | |
| **10** | 60 | 1.375 | 0.030 | 360 | |
| **11** | 20 | 1.610 | 0.090 | 242 | 0.0167 |
| **12** | 20 | 2.190 | 0.180 | 3 | 0.0002 |

For the purposes of the LST algorithm the surface albedo was calculated in the map algebra calculator `r.mapcalc` of GRASS GIS using the Eq.1 and the coefficients $\omega_{bi}$ from Table 9 with the command:

*(Float("B02.tif")*0.1324+Float("B03.tif")*0.1269+Float("B04.tif")*0.1051+Float("B05.tif")* 0.0971+Float("B06.tif")*0.0890+Float("B07.tif")*0.0818+Float("B08.tif")*0.0722)/10000*

The resulting albedo raster layer was resampled to 10 m by cubic convolution. This product is used to approximate the surface emissivity in the proposed algorithm. Figure 20 shows the example of both the albedo and emissivity for the acquisition from 14 September 2016.

Simulation of the cooling effects of the urban greenery requires data on the ***properties of the ground cover material***. We approximated such properties by calculating zonal mean albedo for each ground land cover class after masking the trees and shrubs above 1.5 m high. Furthermore, continuous raster layer of ***albedo of the urban trees*** can be extracted using the urban trees mask and the surface albedo layer (Fig. 21).

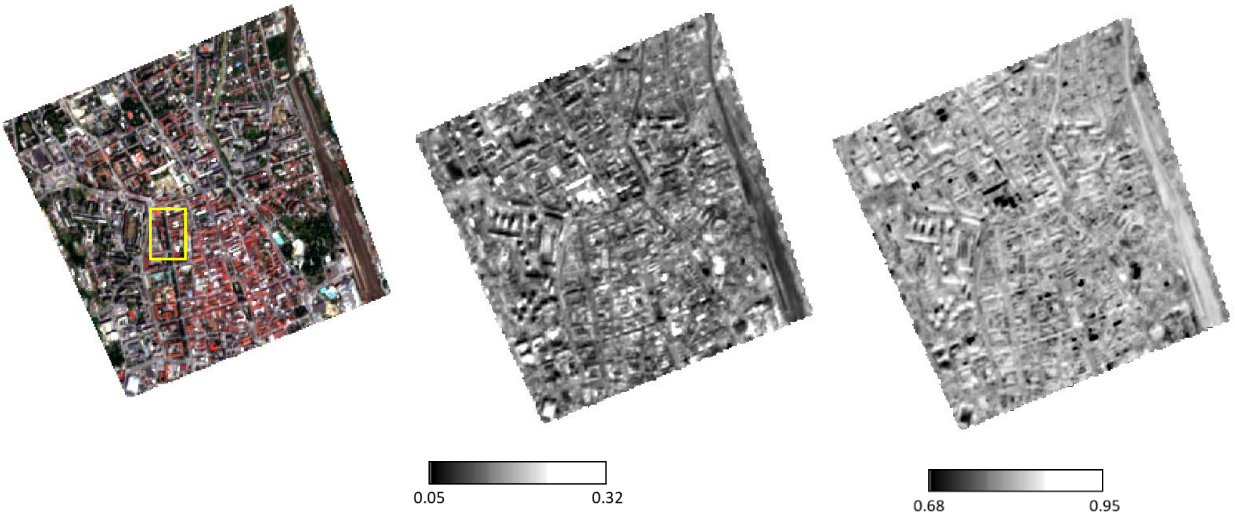


*S2 natural colour composite 10m* | *S2 broad-band surface albedo10m* | *S2 surface emissivity 10m*

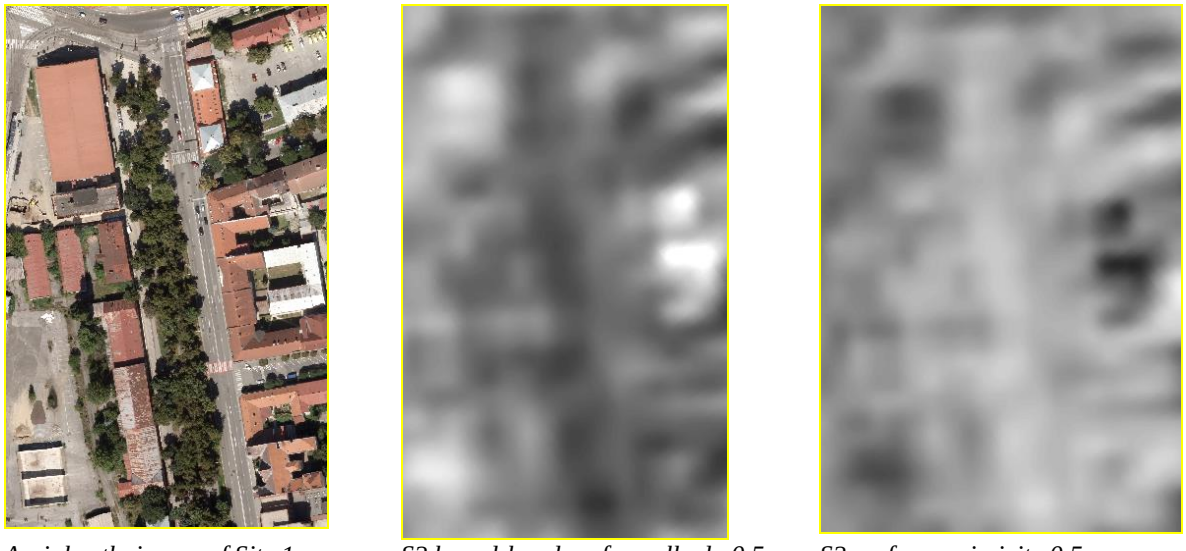

*Aerial orthoimage of Site 1 Moyzesova street as natural colour composite 0.5 m* | *S2 broad-band surface albedo 0.5m* | *S2 surface emissivity 0.5 m*

*Figure 20. Surface albedo and surface emissivity derived from Sentinel 2 Level 1C product for the entire study area (2 by 2 km) and for the site 1 in the detail (yellow outline) for 14 September 2016.*

*Mask of urban greenery as trees and shrubs extracted from ALS and aerial orthoimagery.*

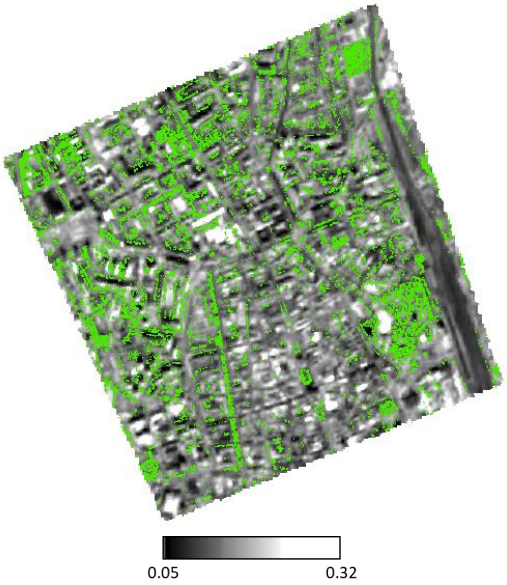


*Surface albedo derived from S2 L1C data overlaid by urban greenery mask*

*Land cover as 20 categories representing the material of the ground below the trees and shrubs.*

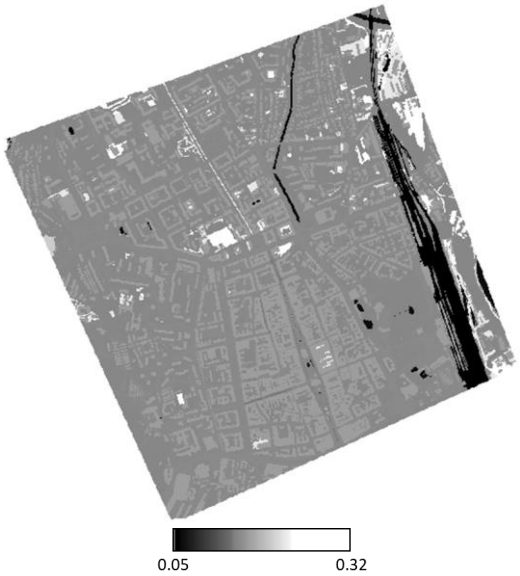


*Ground surface albedo calculated as zonal mean within the ground land cover classes after masking the trees and shrubs*

*Figure 21. Surface albedo derived for different classes of the ground land cover from Sentinel 2 Level 1C product for the entire study area (2 by 2 km) for 14 September 2016.*

***Vegetation transmittance*** of solar radiation to the ground surface was the third product derived from the Sentinel 2 data for our purposes of simulating the cooling effect of urban greenery. The rationale behind was in applying the linear regression models of the estimated leaf area index derived from TLS time series and Sentinel 2 NDVI time series (SURGE_D4_VEGMETR). Figure 12 shows the scatterplots and liner models between the two variables. The spatial coverage represents the spatial extent of the four sites displayed in Fig. 1. The LAI_TLS was calculated at 10 m cell size directly from the TLS point clouds to match the resolution of Sentinel 2 NDVI. For particular date of scanning with TLS, Figure 15 shows cell values of LAI_TLS from all 4 sites binned together and plotted against

corresponding values of S2_NDVI. Apparently, there is no meaningful relationship between the two variables. However, locally there is. For example, site 1 (Moyzesova street) exhibits relatively strong relationship for summer months (Fig. 12). Despite the distribution of the variables around the regression line is very bimodal (clustering of low and high values), we used the linear model for 14 September 2016 and 23 November 2016 to demonstrate how the S2_NDVI could be used to roughly estimate the LAI_TLS to approximate the effect of urban trees solar transmittance (Fig. 12), i.e. to downscale the S2 vegetation metrics to higher resolution urban tree layer. Other indices should be used and more robust approaches statistical exploited to search for a stronger and more convincing linear relationship than the one here presented. Anyway, it can be seen that the effect of leaf-on season is still present in September blocking the sun light while there is the leaf-off season in November. Clearly this is related to the temporal variation in NDVI. The main reason why the NDVI does not correlate with the LAI TLS is very likely in different manner of how the two variables are sensed by the sensor. With TLS the 3D geometry of a tree is very realistically modelled while the vegetation indices derived from passive multispectral satellite sensing of subvertical to vertical field of view capture only reflected radiation from the top parts of the tree canopy. The amount of biomass is thus saturated in the higher NDVI values and also spectral signal of trees is mixed with the ground cover for the cell size relatively larger to the size of an average tree in urban environment. In the site 1, this effect of spectral mixing is probably reduced, i.e. cells values are clean signal from the ground.

### 7.4 Toolbox for modelling the land surface temperature

The SURGE_D5_ALGOSTRUC report comprises the design of the algorithm, i.e. workflow, of how we approached the modelling of the cooling effect taking into account the information extracted from the S2 mutlispectral imagery. Partial outcomes of this workflow are presented as example output data layers for selected days within a year. The summary of results does not contain output layers derived from all acquired input datasets (TLS or S2 data) or all possible scenarios. During this project we have conducted the following steps that lead to our estimation of LST and surface UHIs including the representation of cooling effects of urban greenery in the Košice city:

- creation of a 3D city model representing urban surfaces such as buildings, roads, urban greenery in the form of digital surface model (digital terrain model + buildings + trees) or a full 3D model;
- evaluation and parameterization of trees for effects on solar radiation (shadows, albedo) and heat transfer using lidar and Sentinel data;
- preparation of input data in a vector and raster data formats for solar radiation modelling using r.sun/v.sun for the selected time horizons;
- land surface temperature estimation using Stefan-Boltzmann equation using assessment of solar irradiance and irradiation, land cover parameterization and meteorological data;
- evaluation of various scenarios reflecting a different state of urban greenery using GRASS GIS to assess the best ways to mitigate UHIs.

These steps define these major components of the algorithmic structure for the future toolbox:

1. Data component: 3D city model (vector format), input GIS data (vector/raster), meteo data (vector-point);

2. Simulation/modelling component: r.sun/v.sun solar radiation models a Stefan-Boltzmann land surface temperature model;
3. Prediction component: Based on actual data, the simulation component will produce data on predicted LST, thus providing information on expected LST in any location within the city. Evaluation of various scenarios based on different input data parameters will help to better plan counter UHI measures, such as changing roof colour paintings to increase albedo or planting trees in UHI hotspots.;

The suggested toolbox consists of the following tools implemented in GRASS GIS:

1. Data component: `v.in.gdal, r.in.ascii, r.slope.aspect`
2. Simulation component: `lst.stefan-boltzman.sh, r.sun, v.sun, r.mapcalc`
3. Prediction component: `r.mapcalc`

The workflow used is graphically outlined in Fig. 16. The role of Sentinel 2 data products is highlighted by thick outline. The main contribution of Sentinel 2 data in LST calculation is in the estimation of albedo and thermal emissivity of the land cover surface.

### 7.5 Roadmap for further implementation of the algorithm

The developed algorithmic toolbox can be converted into a more compact kind of tool as plugin for which a roadmap was elaborated. The report SURGE_D5_ALGOSTRUC provides more details for a specialized software toolbox called `r.lst` to be implemented in open-source GRASS GIS. This report summarizes the findings and methods developed within this project. The roadmap proposes a 2-year period for the software development and implementation divided into 3 work packages with several subtasks. These subtasks include software design and coding, software testing and verification using validation datasets and implementation in GRASS GIS. We suggest further development based on the Tangible Landscape concept that should improve the communication and data interaction between user and model leading to increased applicability of the model in urban planning and city management

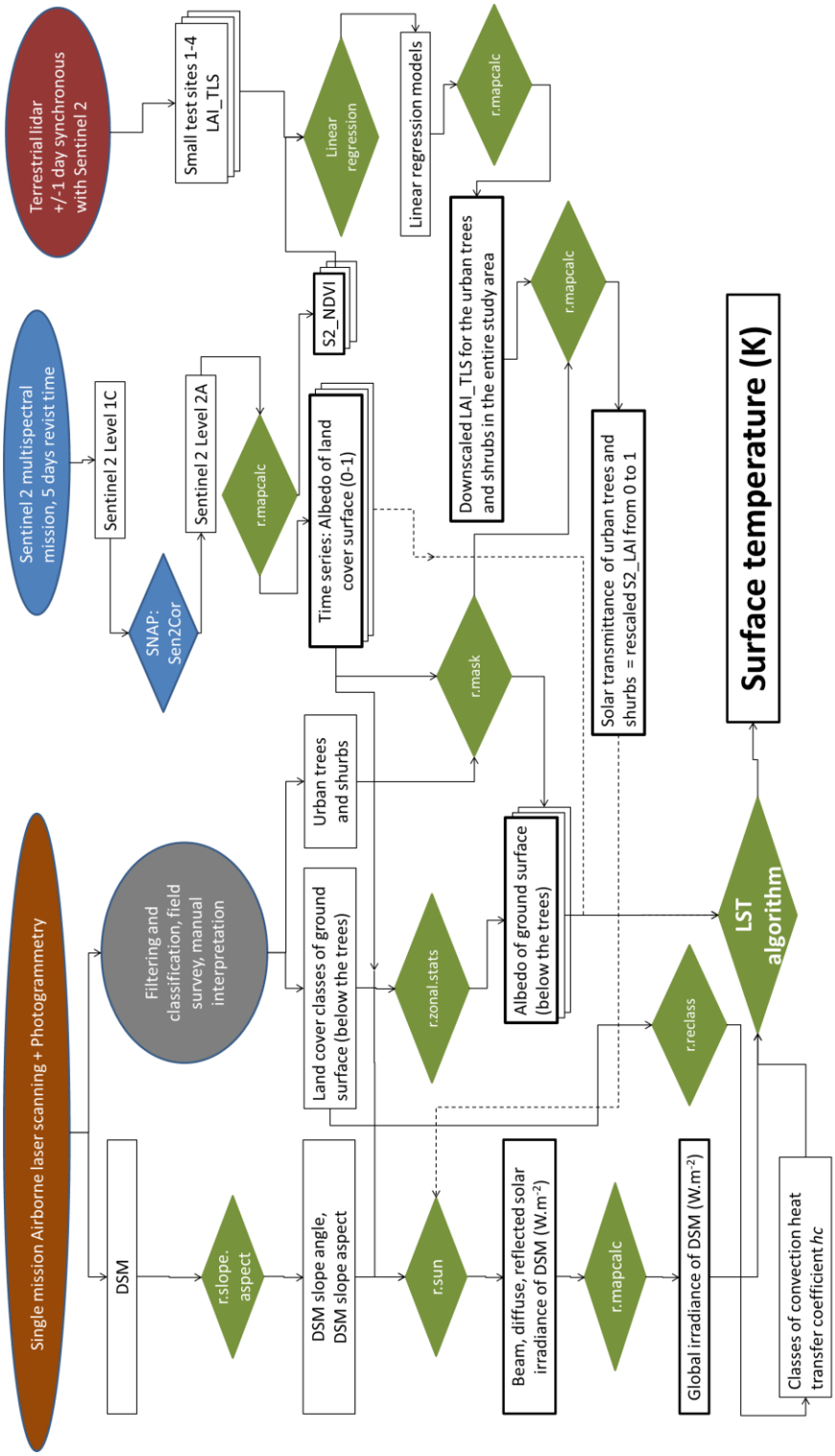


*Figure 22. Schematic workflow of preparing the inputs for the land surface temperature modelling. Elipses denote the data acquisition methods, rectangles denote the data layers or products, pinacoids denote processes. Green colour is marks the processes in the GRASS GIS environment, blue colour marks the SNAP environment for processing Sentinel 2 products. Thick outline marks the data layers derived from Sentinel 2 products.*

# 8 Management of the project

The feasibility study was contracted from June 2016 to May 2018. The activity on the project started earlier, in April 2016 in terms of data acquisition by terrestrial laser scanning and gathering the multispectral imagery. We progress according to the plan set up in the project proposal (Fig. XX) until December 2017 when slippage of the work occurred. The reason was in misunderstanding of the invoicing and reception of payment related to the first use of the ESA-p administration system. We were expecting confirmation from ESA that the first submitted deliverables were going to be accepted. As we have not uploaded the deliverables (documents) to the ESA-p system, the invoice could not be processed. Meanwhile, the uncertainty of accepting the submitted partial results induced delays in further work. This problem was discussed with the representatives of ESA and resolved during the progress meeting in Bratislava in December 2017. Both sides agreed on extension of the project closure to 28 September 2018 and the work plan had been modified (Fig. XX) which we highly appreciated. The modified workplan was met so that the final results could be presented during the progress meeting with ESA representatives in Bratislava (Novemeber 2018) and in ESRIN Frascati (November 2018).

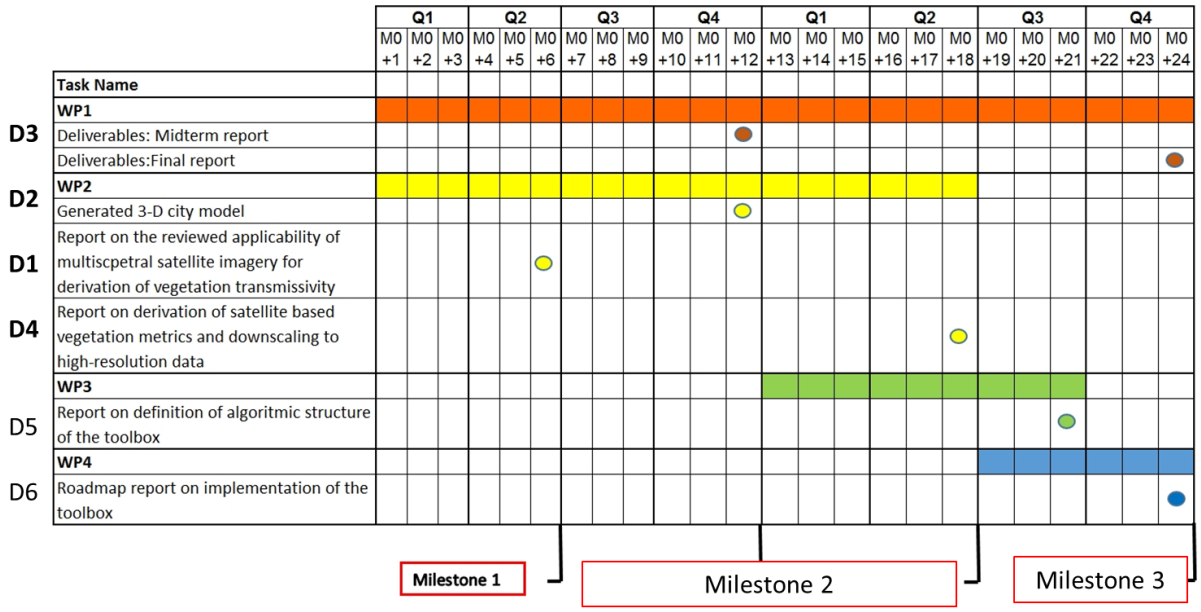


Figure 23. Original work plan

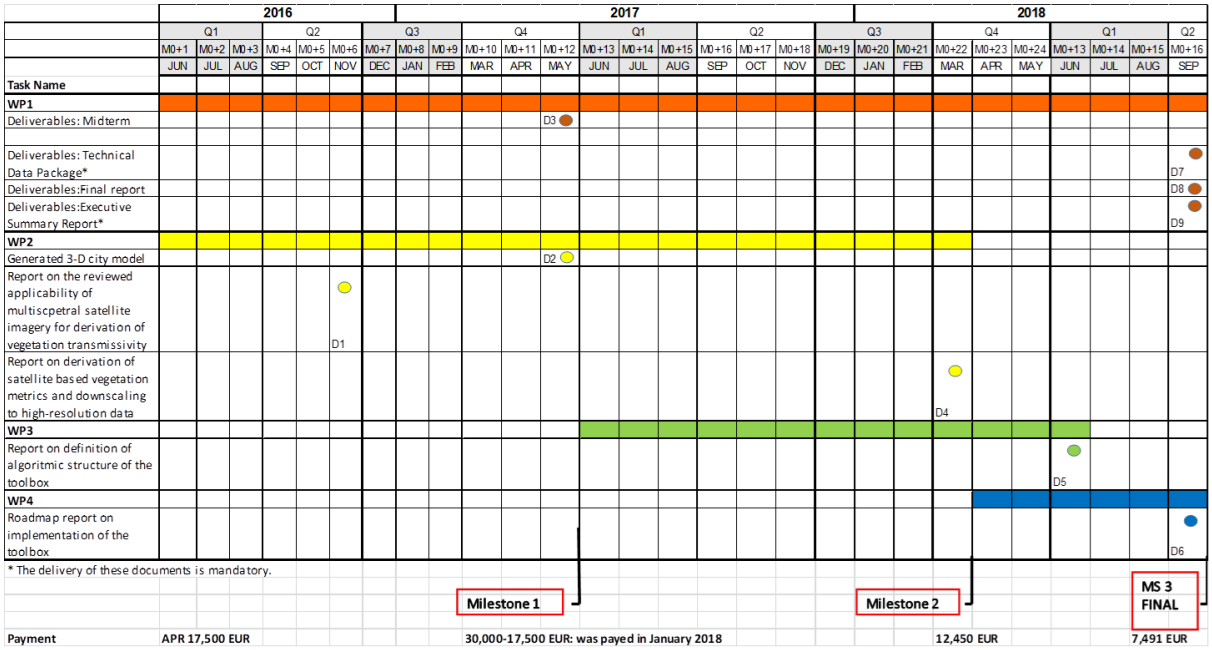

Figure 24. Work plan after extending the study closure

## 8.1 Status of Technical Notes

Table 10 summarizes the activities and deliverables with associated months of their submission.

*Table 10. Summary of the status of activities and associated technical notes*

| **Work package / Responsible person** | **Activities/Tasks** | **Status** | **Date due** |
|---|---|---|---|
| **WP1: Study management** Jaroslav Hofierka | Meetings of the project team | Finished | Sept. 2018 |
| | WP1 Progress report 1<br>WP1 Progress report 2 Mid-term (D3)<br>WP1 Progress meeting Bratislava<br>WP1 Progress report 3+4<br>WP1 Progress meeting Bratislava<br>WP1 Final meeting ESRIN, Frascati, Rome<br>WP1 Technical data Package (D7)<br>WP1 Final report (D8)<br>WP1 Executive summary report (D9) | Finished | Dec. 2016<br>June 2017<br>Dec. 2017<br>May 2018<br>Nov. 2018<br>Nov. 2018<br>Nov. 2018<br>Nov. 2018<br>Nov. 2018 |
| **WP2: Data, methods and architecture of the system** Michal Gallay | Review of the state-of-the-art on vegetation transmittance (**D1**) | Finished | Dec. 2016 |
| | Generated 3D city model (**D2**) | Finished | May 2016 |
| | Generation of 3D time series of urban greenery | Finished | Sep. 2017 |
| | Gathering of Sentinel 2A imagery | Finished | Dec. 2017 |

| | | | |
|---|---|---|---|
| | Preparing input data for 3D solar modelling | Finished | March 2018 |
| | Report on derivation of satellite based vegetation metrics and downscaling to high-resolution data (**D4**) | Finished | April 2018 |
| **WP3 - Testing, validation and viability of the system/model** Jaroslav Hofierka | Report on definition of algorithmic structure of the toolbox (**D5**) | Finished | Sept. 2018 |
| **WP4 - Roadmap for further implementation** Jaroslav Hofierka | Roadmap report on implementation of the toolbox (**D6**) | Finished | Sept. 2018 |

## 8.2 Derived publications

The research conducted within the SURGE study was partially published in the following publications :

1. HOFIERKA, J., GALLAY, M., KAŇUK, J., ŠUPINSKÝ, J., ŠAŠAK, J. (2017). High-resolution urban greenery mapping for micro-climate modelling based on 3D city models. The International Archives of the Photogrammetry, Remote Sensing and Spatial Information Sciences (***ISPRS Archives***), XLII-4/W7, 7-12. (3D Geoinfo Conference, Melbourne, Australia)
2. KAŇUK, J., GALLAY, M., HOFIERKA, J., ŠAŠAK, J., ŠUPINSKÝ, J., SEDLÁK, V., GESSERT, A., 2017. Monitoring dynamics of urban greenery for more accurate solar radiation mdoelling in urban landscape. In: Inspektor, T., Horák, J., Růžička, J. (Eds.) ***Symposium GIS Ostrava 2017***, Geoinformatika v pohybu, 22. - 24. March 2017. VŠB - Technická univerzita Ostrava, Czech Republic.
3. ONAČILLOVÁ, K., GALLAY, M. 2018. Spatio-temporal analysis of surface urban heat island based on LANDSAT ETM+ and OLI/TIRS imagery in the city of Košice, Slovakia. ***Carpathian Journal of Earth and Environmental Sciences***. 13(2), 395 - 408.
4. ONAČILLOVÁ, K., GALLAY, M. 2018 : Analysing relation of vegetation metrics derived from Sentinel 2 data and laser scanning data. ***GIS Ostrava 2018***.
5. HOFIERKA, GALLAY, ... 2019: New tool for physically based land surface temperature modelling in GIS. *Computers and Geosciences*. In preparation.

# 9 Conclusion

The interaction of incoming solar radiation with urban surfaces is the main source of heat energy inducing urban heat islands within a city. Land surface temperatures within the city exhibit great spatial variations that can be modelled by proper software tools and input data such as Sentinel 2A. Spatial distribution of solar energy income can be modelled based on physical and geometric principles in a relatively straightforward and accurate way. Tools enabling spatially distributed solar modelling are available in contemporary GIS, but no such tools exist to convert the calculated solar energy income into land surface temperature (LST).

The open-source GRASS GIS comprises one of the most robust tools for solar irradiation modelling such as r.sun on which the members of the SURGE project team collaborated in the past. We used r.sun as a base for calculating the solar energy income and we developed an algorithm based on the Stefan-Boltzmann Law, which describes the power radiated from a black body in terms of its temperature. The key inputs of the LST calculation comprise spatially distributed global solar irradiation of a DSM, convective heat transfer coefficient of the surface material, albedo of the surface and the emissivity of the material. While solar energy income can be calculated with a high degree of reliability, the latter three parameters are difficult to be measured directly by remote sensing instruments in such a fine resolution as the solar irradiation can be computed.

We have demonstrated that Sentinel 2 data can be used in the procedure for LST calculation, particularly in estimating the broad-band albedo, surface material emissivity and urban trees transmittance. In regard to the latter variable, we have tested the NDVI derived from Sentinel 2 data products as a proxy for ascertaining the transmittance of solar energy by urban trees and shrubs. Time series of TLS point clouds were used to parametrize the transmittance by estimated LAI. However, it seems linear regression models do not sufficient to describe this relationship between S2 NDVI and TLS LAI and the linear correlation is weak to moderate. We see another reason for which the linear relationship could not be specified in the modifiable area unit problem as the S2 grid cells are coarse 2D spatial units with respect to 3D points of much higher density. Further testing and more robust geostatistical approaches need to be exploited to describe the relationship more tightly should it exist. Despite this shortcoming, the functionality of the developed toolbox was demonstrated. The proposed approach can be used for testing on any other geographical area or city providing that the following datasets exist: gridded DSM, land cover classification, land cover of the ground (below the trees), spatially distributed broad-band albedo, e.g. from Sentinel 2 data products, convective heat transfer coefficient, ambient air temperature, equilibrium surface temperature, and effective radiant sky temperature.

The proposed approach provides means for GIS specialists and urban planners to assess and communicate the impact of measures taken in order to mitigate the urban heat island or communicate the effect of greenery on cooling the urban climate. However, the approach requires further testing in terms of validating the calculated temperature values in respect to more reliable data sets or methods. This aspect is to be discussed in the roadmap for a developing a GRASS GIS module for simulating the land surface temperature using the methodology developed in the SURGE project. The open-source concept of GRASS GIS will stimulate further development of the module and stimulate a wider use of the module including the data form ESA sensors such as Sentinel 2.

# References

ASHRAE (1989). Handbook Fundamentals, American Society of Heating, Refrigeration, and Air-Conditioning Engineers, Atlanta, Georgia.

Algarni, S. A. (2015). Modeling Radiation Heat Transfer for Building's Cooling and Heating Loads: Considering the Role of Clear, Cloudy, and Dusty Conditions in Hot and Dry Climates.Theses and Dissertations. 1231.

Alonzo, M., Bookhagen, B., McFadden, J.P., Sun, A., Roberts, D.A. (2015). Mapping urban forest leaf area index with airborne lidar using penetration metrics and allometry. Remote Sens. Environ., 162, pp. 141-153.

Amir, A.K., Katoh, Y., Katsurayama, H., Koganei., M., Mizunuma, M. (2018). Effects of convection heat transfer on Sunagoke moss green roof: A laboratory study. Energy and Buildings 158, 1417-1428.

Berdahl, P., Bretz, S. E. (1997). Preliminary survey of the solar reflectance of cool roofing materials. Energy and Buildings, 25, 149-158.

Bonafoni, S., Anniballe, R., Gioli, B., Toscano, P. (2016). Downscaling Landsat Land Surface Temperature over the urban area of Florence. European Journal of Remote Sensing, 49(1), 553-569.

Bretz, S., Akbari, H., Rosenfeld, A. (1998). Practical issues for using solar-reflective materials to mitigate urban heat islands. Atmospheric Environment, 32, 95-101.

Dubayah, R., Rich, P. M. (1995). Topographic solar radiation models for GIS. International Journal of Geographical Information Systems 9: 405-19

D'Urso, G., Calera, A. (2006). Operative approaches to determine crop water requirements from earth observation data: methodologies and applications. AIP Conf. Proc., 852 (2006), pp. 14-25

EPA, 2008. Reducing urban heat islands: Compendium of strategies. U.S. Environmental Protection Agency. https://www.epa.gov/heat-islands/heat-island-compendium.

Fogl, M., Moudrý, V., 2016. Influence of vegetation canopies on solar potential in urban environments. Applied Geography, 66, pp. 73 - 80.

Gallay, M., Kaňuk, J., Hochmuth, Z., Meneely, J., Hofierka, J., Sedlák, V., 2015. Large-scale and high-resolution 3-D cave mapping by terrestrial laser scanning: a case study of the Domica Cave, Slovakia. International Journal of Speleology, 44(3), pp. 277-291.

Hofierka, J. (1997). Direct solar radiation modelling within an open GIS environment. In Proceedings of the 1997 Joint European GI Conference, Vienna, Austria, 575–584.

Hofierka, J., Zlocha, M. (2012). A New Solar Radiation Model for 3-D City Models. Transactions in GIS, 16, pp. 681-690.

Neteler, M., Mitasova, H. (2004). Open Source GIS: A GRASS GIS Approach. Second Edition. Boston, Kluwer Academic Publishers.

Klingberg, J., Konarska, J., Lindberg, F., Johansson, L., Thorsson, S. (2017). Mapping leaf area of urban greenery using aerial LiDAR and ground-based measurements in Gothenburg, Sweden. Urban Forestry and Urban Greening. 26 (2017). pp. 31-40.

Liu, J., Heidarinejad, M., Graci, S., Srebric, J. (2015). The impact of exterior surface convective heat transfer coefficients onthe building energy consumption in urban neighborhoods withdifferent plan area densities. Energy and buildings, 86, 449-463.

Mirsadeghi, M., Costola, D., Blocken, B., Hensen, J.L.M. (2013). Review of external convective heat transfer coefficient models in building energy simulation programs: implementation and uncertainty, Applied Thermal Engineering, 56, 134–151.

Nichol, J.E., 1994. A GIS-Based Approach to Microclimate Monitoring in Singapore's High-Rise Housing Estates. Photogrammetric Engineering and Remote Sensing, 60, 1225-1232.

Richardson, J.J., Moskal, L.M., Kim, S.H. (2009). Modeling approaches to estimate effective leaf area index from aerial discrete-return LIDAR. Agric. For. Meteorol., 149, pp. 1152-1160.

Smith, M.W., 2016. 2.1.5. Direct acquisition of elevation data: Terrestrial Laser Scanning. In: Clarke, L. (Ed.) Geomorphological Techniques (Online Edition). London: British Society for Geomorphology. http://www.geomorphology.org.uk/sites/default/files/chapters/2.1.5_TLS.pdf

SURGE_D1_SOA_MSVT 2016. Report on the reviewed applicability of multispectral satellite imagery. Internal document submitted as the output of the contracted SURGE study.

SURGE_D4_VEGMETR 2018. Deliverable 4 under WP2: Report on derivation of satellite based vegetation metrics and downscaling to high-resolution data. Internal document submitted as the output of the contracted SURGE study.

SURGE_D5_ALGOSTRUC 2018. Deliverable 5 under WP3: Report on definition of algorithmic structure of the toolbox. Internal document submitted as the output of the contracted SURGE study.

SURGE_D6_ROADMAP 2018. Deliverable 6 under WP4: Roadmap report on implementation of the toolbox. Internal document submitted as the output of the contracted SURGE study.

SURGE_PR1 2016. Progress report 1. Internal document submitted as the output of the contracted SURGE study.

SURGE_PR2 2017. Progress report 2 Mid-term report. Internal document submitted as the output of the contracted SURGE study.

SURGE_PR4 2018. Progress report 4 (merged report 3 and 4). Internal document submitted as the output of the contracted SURGE study.

Šúri, M., Huld, T.A., Dunlop, E.D. (2005). PVGIS: a web-based solar radiation database for the calculation of PV potential in Europe. International Journal of Sustainable Energy 24, 55–67.

Tooke, T.R., Coops, N.C., Goodwin, N.R., Voogt, J.A., 2009. Extracting urban vegetation characteristics using spectral mixture analysis and decision tree classifications. Remote Sensing of Environment, 113(2), pp. 398 - 407.

Tooke, T.R., Coops, N.C., Voogt, J.A., Meitner, M.J., 2011. Tree structure influences on rooftop-received solar radiation. Landscape and Urban Planning, 102 (2), pp. 73 - 81.

Tooke, T.R., Coops, N.C. Christen, A., Gurtuna, O., Prévot, A., (2012). Integrated irradiance modelling in the urban environment based on remotely sensed data. Solar Energy, 86(10), pp. 2923-2934.

Trochta, J., Krůček, M., Vrška, T., Král, K., 2017. 3D Forest: An application for descriptions of three-dimensional forest structures using terrestrial LiDAR. PLoS ONE, 12 (5), e0176871.

Vanino, S., Nino, P., De Michele, C., Bolognesi, S. F., D'Urso, G., Di Bene, C., Pennelli, B., Vuolo, F., Farina, R., Pulighe, G., Napoli, R. (2018). Capability of Sentinel-2 data for estimating maximum evapotranspiration and irrigation requirements for tomato crop in Central Italy, Remote Sensing of Environment, 215, 452-470.

Vollaro, A., Galli, G., Vallati, A. (2015). CFD Analysis of Convective Heat Transfer Coefficient onExternal Surfaces of Buildings. Sustainability, 7, 9088-9099.